Published in final edited form as:
Front Biosci (Landmark Ed). ; 15: 661–680.

Modeling calcium waves in cardiac myocytes: importance of calcium diffusion

Pawel Swietach[1], **Kenneth W Spitzer**[2], and **Richard D Vaughan-Jones**[1]

[1]Burdon Sanderson Cardiac Science Centre, Department of Physiology, Anatomy and Genetics, Oxford OX1 3PT, UK

[2]Nora Eccles Harrison Cardiovascular Research and Training Institute, University of Utah, Salt Lake City, USA

Abstract

Under certain conditions, cardiac myocytes engage in a mode of calcium signaling in which calcium release from the sarcoplasmic reticulum (SR) to myoplasm occurs in self-propagating succession along the length of the cell. This event is called a calcium wave and is fundamentally a diffusion-reaction phenomenon. We present a simple, continuum mathematical model that simulates calcium waves. The framework features calcium diffusion within the SR and myoplasm, and dual modulation of ryanodine receptor (RyR) release channels by myoplasmic and SR calcium. The model is used to illustrate the effect of varying RyR permeability, sarco/endoplasmic reticulum Ca^{2+} ATPase (SERCA) activity and calcium ion mobility in myoplasm and SR on wave velocity. The model successfully reproduces calcium waves using experimentally-derived variables. It also supports the proposal for wave propagation driven by the diffusive spread of myoplasmic calcium, and highlights the importance of SR calcium load on wave propagation.

Keywords

Calcium; waves; Diffusion; Modeling; Myocyte; Heart; Cardiac; Sarcoplasmic Reticulum

2. INTRODUCTION

Intracellular Ca^{2+} waves are a form of Ca^{2+} signaling executed in many cell types (1). Ca^{2+} waves can occur in cardiac myocytes that have been 'Ca^{2+} overloaded' (2, 3). The appearance of waves is usually arrhythmogenic, as it activates inward currents such as that carried by Na^{+}-Ca^{2+} exchange (NCX) (4). Waves are produced as a consequence of Ca^{2+} release through ryanodine receptor (RyR) channels expressed in the sarcoplasmic reticulum (SR), the myocyte's reservoir of stored Ca^{2+}. These release events do not occur simultaneously throughout the cell, but are triggered in succession, one release event acting as the trigger for an adjacent release event. After release, Ca^{2+} is taken back into the SR by the SERCA pump. The nature of this propagating mechanism means that a wave travels at a finite velocity. This is therefore dissimilar to the Ca^{2+} transient evoked by an action potential, which is a whole-cell release event, coordinated by depolarization-activated Ca^{2+} entry through L-type Ca^{2+} channels (5). Ca^{2+} diffusion inside myocytes is clearly a major factor that will determine Ca^{2+} wave velocity. Wave velocity, in turn, will determine the pace of Ca^{2+} release: faster velocity will produce a more coordinated release and a higher

Send correspondence to: Professor Richard D. Vaughan-Jones, Address: Burdon Sanderson Cardiac Science Centre, Department of Physiology, Anatomy and Genetics, Oxford OX1 3PT, UK, Tel: 0044 1865 272451, Fax: 0044 1865 272451, richard.vaughan-jones@dpag.ox.ac.uk.

Europe PMC Funders Author Manuscripts

myoplasm-averaged rise in [Ca^{2+}], which will exert a greater effect on membrane potential and contractile state.

In this study, we present a simple mathematical framework for understanding the importance of Ca^{2+} ion diffusion in the propagaton Ca^{2+} waves, with particular emphasis on their velocity, a readily-measureable wave parameter. Our spatial model features a continuum diffusion-reaction representation of free and buffered Ca^{2+} ions in both myoplasm and SR (6), and also incorporates a simplified (non-Markovian) but comprehensive representation of RyR channel modulation by myoplasmic and SR [Ca^{2+}] (7-11). With these features, the model provides a first attempt at reconciling recent work on Ca^{2+} mobility with the mechanism for Ca^{2+} wave propagation.

2.1. Calcium mobility

The calcium ion is highly reactive and binds readily to buffer sites within cells. These buffer sites are held on large molecules, such as troponin in the myoplasm, and calsequestrin in the SR, as well as smaller molecules such as calmodulin and ATP (6, 10, 12). In myoplasm during diastole, it is estimated that only one in a thousand Ca^{2+} ions remains unbound (12, 13). This ratio is believed to be closer to one in ten for Ca^{2+} within the SR (6, 14). Figure 1 shows buffering capacity curves determined empirically for the myoplasm (13, 15, 16) and SR (14). Since most Ca^{2+} buffering is hosted by molecules considerably larger than the Ca^{2+} ion, effective Ca^{2+} ion mobility is predicted to be low. Overall Ca^{2+} mobility is the sum of free Ca^{2+} ion diffusion and buffered Ca^{2+} (buf) diffusion (17):

$$\frac{\partial Ca}{\partial t}+\frac{\partial buf}{\partial t}=D_{free}\cdot\frac{\partial^2 Ca}{\partial x^2}+D_{buf}\cdot\frac{\partial^2 buf}{\partial x^2}$$

This equation can be simplified using the chain rule,

$$\frac{\partial buf}{\partial t}=\frac{\partial buf}{\partial Ca}\cdot\frac{\partial Ca}{\partial t};\frac{\partial buf}{\partial x}=\frac{\partial buf}{\partial Ca}\cdot\frac{\partial Ca}{\partial x}$$
$$\therefore\ \frac{\partial Ca}{\partial t}\cdot\left(1+\frac{\partial buf}{\partial Ca}\right)=\left(D_{free}+D_{buf}\cdot\frac{\partial buf}{\partial Ca}\right)\cdot\frac{\partial^2 Ca}{\partial x^2}$$

In unbuffered media at 37°C, the diffusion coefficient for *free* Ca^{2+} (D_{free}) is ~1000μm^2/s (18). However, in the presence of a non-diffusible buffer (concentration C and Ca^{2+} dissociation constant K), effective Ca^{2+} mobility (D_{eff}) is given by:

$$D_{eff}=D_{free}\cdot\left(1+\frac{C\cdot K}{\left(K+\left[Ca^{2+}\right]\right)^2}\right)^{-1}\quad\text{Eq 1}$$

Ca^{2+} mobility can be facilitated by parallel diffusion of Ca^{2+}-bound, low molecular weight buffers. Such ‘facilitated diffusion’ also underpins cytoplasmic mobility of the H^+ ion (19), another example of a buffered ionic species. To account for facilitated diffusion aboard buffers, Eq 1 can be expanded to include several buffers, each with a diffusion coefficient D:

$$D_{eff}=\frac{D_{free}+\sum_i^N\frac{D_i\cdot C_i\cdot K_i}{(K_i+[Ca^{2+}])^2}}{1+\sum_i^N\frac{C_i\cdot K_i}{(K_i+[Ca^{2+}])^2}}\quad\text{Eq 2}$$

Overall mobility can be reduced further by tortuosity due to geometrical restrictions and/or macromolecular crowding. This factor has been estimated to reduce ionic mobility by a factor of two in myoplasm (20) and over an order of magnitude in the SR (6). To account for tortuosity, Eq 2 should be scaled by a constant.

Theoretical considerations, based on buffering and tortuosity, predict low effective Ca^{2+} mobility ($D_{eff}<<D_{free}$) in both myoplasm and SR. Experimental measurements have confirmed these predictions. Myoplasmic D_{eff} (D_{Meff}), estimated at diastolic levels of $[Ca^{2+}]$, is ~10-20$\mu m^2/s$ (20-22). Comparable estimates have been made for the cytoplasm of non-muscle cells (23, 24). A key precautionary measure that must be considered in such studies is the propensity for exogenous buffers (such as Ca^{2+} fluorophores, if present) to inflate D_{Meff} artefactually (24). Low myoplasmic Ca^{2+} mobility is consistent with the local nature of Ca^{2+} signaling in myocytes, within functional 'units' called couplons (5, 25). The fundamental SR release event is a Ca^{2+} spark (first described in (26)) which may involve simultaneous activation of a cluster of ~20 RyR channels (26). During this non-propagating SR release event, myoplasmic $[Ca^{2+}]$ rises to 200-300nM within ~10ms over a 2μm-wide space. Sustaining such a steep concentration gradient over a small distance requires Ca^{2+} to diffuse slowly (25). In isolation, such an event does not produce a contractile response. However, coordinated opening of tens of thousands of RyRs will generate sufficient Ca^{2+} to engage the contractile apparatus throughout the myocyte. Low Ca^{2+} mobility also ensures that the response can be graded by varying the number of activated release sites. However, in order to reach contractile proteins, Ca^{2+} must be adequately mobile. A mobility of 10-20$\mu m^2/s$ is a compromise between localization of Ca^{2+} signaling and Ca^{2+} penetrability into the myoplasm.

Two recent studies have tackled the issue of SR D_{eff} (D_{SReff}). As expected from SR luminal buffering and tortuosity, D_{SReff} was found to be lower than free Ca^{2+} mobility, D_{free}. The first study suggested a mobility of 60$\mu m^2/s$ at room temperature (~80$\mu m^2/s$ when corrected to 37°C) (27), i.e. considerably faster than myoplasmic Ca^{2+} mobility. However, the second study (6) estimated D_{SReff} to be 9$\mu m^2/s$ i.e. of similar order of magnitude to myoplasmic D_{eff}. The difference between these two studies may represent species differences (rabbit in (27) vs rat and guinea-pig in (6)), but it may also be explained by experimental design. The first study (27) measured relaxation of an intra-SR $[Ca^{2+}]$ gradient, imposed by a transient and local exposure to caffeine to empty SR regionally. The relaxation time-course was measured using an intra-SR Ca^{2+} dye (Fluo-5N), and fitted with diffusion equations to obtain mobility. The second study (6) used a caffeine-based protocol to empty the SR at one end of the cell and, after a delay, empty the remainder of the SR. SR content was assayed using measurements of myoplasmic $[Ca^{2+}]$, made under conditions that control for background SR leak, SR uptake and sarcolemmal transport. These experiments showed that SR Ca^{2+} mobility is similar to, or even smaller than myoplasmic Ca^{2+} mobility. Incidentally, when background SR leak was not allowed for, a much larger value for D_{SReff} was obtained, emphasizing the importance of controlling 'reaction' fluxes in diffusion-reaction phenomena, whenever the mathematics are simplified to a diffusive problem (6).

The exact value of D_{SReff} remains an actively researched and hotly debated topic (25, 28). It is noteworthy, however, that the lower estimate for D_{SReff} is in agreement with the rate of 'Ca^{2+} blink' recovery (29, 30) i.e. the relaxation of intra-SR $[Ca^{2+}]$ non-uniformity following a Ca^{2+} spark, the kinetics of which are believed to be diffusion-limited (31). Low SR Ca^{2+} mobility is also in agreement with the paradigm of local Ca^{2+} signaling. If D_{SReff} were larger than D_{Meff}, individual release sites would no longer be independent (25) because depletion at one site would promptly and significantly reduce the substrate for release elsewhere. To summarize, Ca^{2+} mobility in myoplasm and the SR have been shown, both

experimentally and theoretically, to be much lower than free Ca^{2+} ion mobility in unbuffered medium.

2.2. Calcium waves

Intracellular Ca^{2+} waves were first inferred from spontaneous contractions observed under conditions of elevated [Ca^{2+}] in skinned cardiac cells (32), and later in intact cells (33). With the advent of high-resolution imaging, Ca^{2+} waves were described as Ca^{2+} release events that propagate throughout the cell at constant velocity (3, 34). In cardiac myocytes, velocity has been estimated to be ~100μm/s (35).

The fundamental event that triggers a Ca^{2+} wave is a local Ca^{2+} release that, under a special set of conditions, elicits Ca^{2+} release from adjacent SR regions (Figure 2A). RyR channels are central to Ca^{2+} wave propagation, as they are sensitive to myoplasmic [Ca^{2+}] (35, 36) and SR [Ca^{2+}] (37, 38). The initial stimulus for RyR activation could be elevated myoplasmic [Ca^{2+}] (39) or overloaded SR (40), or both.

According to 'classical' models of wave propagation, the Ca^{2+} wave is driven forward by Ca^{2+} diffusion in the myoplasm (Figure 2B). Under this hypothesis, the myoplasmic Ca^{2+} wavefront will travel ahead of any SR Ca^{2+} wavefront. Recently, an alternative model of Ca^{2+} wave propagation (41) has been postulated. In this model, a Ca^{2+} wave arises as a result of the spread of an intra-SR Ca^{2+} overload that sensitizes RyR channels *en route* (Figure 2C). Ca^{2+} released into the myoplasm is resequestered back into the SR by SERCA pumps. The activity of these pumps raises intra-SR [Ca^{2+}] locally. This 'bolus' of SR Ca^{2+} spreads diffusively and sensitizes downstream RyR channels, so that a rise in myoplasmic [Ca^{2+}] opens RyRs more readily. Under this proposal, Ca^{2+} diffusion in the SR cannot be slower than in the myoplasm (27), i.e. the SR wavefront of RyR sensitization must travel ahead of the myoplasmic Ca^{2+} wavefront. In addition, a local rise in SR [Ca^{2+}] is expected to precede the myoplasmic [Ca^{2+}] wave. For either model, the propagation velocity will depend on

- **i.** the distance between adjacent release sites,
- **ii.** the time taken for RyR channels to open.

These parameters are somewhat analogous to the length and time constants of membranes, which determine the velocity of action potential propagation in axons (42). An upper limit for the greatest spacing σ between adjacent release sites can be estimated by comparing Ca^{2+} wave velocity (v_{Ca}) with the Ca^{2+} diffusion coefficient (D_{eff}). The time taken for Ca^{2+} to diffuse distance σ must be shorter than the time-delay expected from the wave velocity, i.e.

$$\frac{\sigma^2}{2 \cdot D_{eff}} < \frac{\sigma}{v_{Ca}} \quad \text{Eq 3}$$

It is important to note that the next adjacent release site must contain activatable RyR channels *and* sufficient substrate (i.e. SR [Ca^{2+}] content) for release. Under such a model, fast Ca^{2+} wave velocity is favored by:

- **i.** fast myoplasmic Ca^{2+} diffusion,
- **ii.** low RyR activation threshold,
- **iii.** rapid Ca^{2+} release,
- **iv.** an adequate SR Ca^{2+} store in adjacent regions.

It is clear from the postulated models of Ca^{2+} wave propagation that Ca^{2+} mobility in both SR and myoplasm must play a major role in setting Ca^{2+} wave velocity. Ca^{2+} mobility will also affect RyR channel modulation by Ca^{2+} ions on both the myoplasmic and luminal SR side. For instance, the local SR [Ca^{2+}] load that modulates RyR channels will depend on the extent to which intra-SR Ca^{2+} has diffused, following a local release event elsewhere in the SR (6). Similarly, the dilution of myoplasmic [Ca^{2+}] by diffusion will affect the rate at which the RyR opening threshold is reached, the time-course of channel inactivation, and the transmembrane Ca^{2+} gradient.

Mathematical models have been instrumental in our understanding of Ca^{2+} waves (43-47). To understand the importance of Ca^{2+} diffusion in determining Ca^{2+} wave velocity, we have constructed a simple continuum diffusion-reaction model. Our model allows for intra-SR Ca^{2+} diffusion and incorporates RyR modulation by both *cis* and *trans* [Ca^{2+}]. The simplicity of the model renders it useful for didactic purposes, and for testing hypotheses for Ca^{2+} wave propagation.

3. METHODS

3.1. Measuring calcium mobility and calcium waves

Ventricular myocytes were isolated from rat hearts by a combination of mechanical and enzymic dispersion (see (6) for further details). All procedures were performed in line with UK Home Office regulations. Myocytes were loaded with the acetoxymethyl ester of the Ca^{2+}-sensitive fluorophore Fluo-3 (10μM) and imaged in linescan mode along the myocyte's long-axis under an inverted Leica IRBE microscope coupled to a Leica TCS NT confocal system (detecting fluorescence >515nm). Excitation at 488nm was provided by an argon laser. Fluorescence was reported as a pseudo-ratio F/F_0, normalized to starting fluorescence F_0. Cells were paced at 2Hz and superfused in a Perspex chamber at 37°C with normal Tyrode solution at pH 7.4, containing 135mM NaCl, 4.5mM KCl, 20mM Hepes, 2mM $CaCl_2$, 1mM $MgCl_2$ and 10mM glucose.

To assess Ca^{2+} diffusion in the myoplasm and SR, pacing was stopped and cells superfused with 'solution A' (0Na-0Ca): 140mM *N*-methyl-D-gluconate, 4.5mM KCl, 1mM $MgCl_2$, 10mM glucose, 0.5mM EGTA, 10μM cyclopiazonic acid (CPA, a SERCA inhibitor) and 0.3mM tetracaine (an RyR channel blocker). Under these conditions, the myocyte SR store was stabilized and sarcolemmal fluxes minimized (6). After 30s, one half of the myocyte was exposed to 'solution B' which was similar to 'solution A', but contained 10mM caffeine (RyR activator) instead of tetracaine. The other half of the cell remained exposed to 'solution A' (step 1 in Figure 3Ai). Sharp separation of the two solutions was possible with a dual microperfusion apparatus (6, 19). This maneuver evokes rapid Ca^{2+} release through RyR channels located in the caffeine-exposed part of the myocyte. SR Ca^{2+} release can be estimated from the myoplasmic Fluo-3 signal. After a 30s delay, the entire myocyte was exposed to 'solution B' (step 2 in Figure 3Ai). This maneuver evokes rapid Ca^{2+} release from the remainder of the cell. Details of this method have been validated and published elsewhere (6).

Myoplasmic Ca^{2+} mobility can be assessed from the spread of Ca^{2+} following the first, localized caffeine exposure (step 1 in Figure 3Ai). In the same cell, SR Ca^{2+} mobility can be derived from the relationship between the size of the F/F_0 rise during the localized caffeine exposure (step 1 in Figure 3Ai) versus the response evoked distally by whole-cell caffeine exposure (step 2 in Figure 3Ai). The latter will depend on the extent to which the SR has been drained by the first, localized caffeine pulse.

To trigger Ca^{2+} waves, pacing was stopped and cells were superfused with normal Tyrode solution containing elevated $CaCl_2$ at 7.5mM. Under these conditions, the SR is overloaded and the incidence of Ca^{2+} waves is greatly enhanced (40).

3.2. Mathematical model for calcium waves

One output of the Ca^{2+} wave model is a prediction of wave velocity under different experimental conditions. Our model is a continuum representation, featuring two compartments, the myoplasm (volume fraction v_{myo}) and SR (volume fraction v_{SR}) within which Ca^{2+} diffuses, with effective diffusion coefficients D_{Meff} and D_{SReff}, respectively. Myoplasmic Ca^{2+} is buffered by a fast, lumped myoplasmic buffer (flux J_{Mbuf}), described in (16). SR Ca^{2+} is buffered by calsequestrin (flux J_{SRbuf}), characterized in (14). To simplify the model, Ca^{2+} diffusion coefficients were set to a particular constant, independent of $[Ca^{2+}]$. Indeed, few data are available to characterize fully the $[Ca^{2+}]$-dependence of Ca^{2+}-mobility. Ca^{2+} flux between the two compartments is mediated by SERCA (J_{SERCA}) working in forward or reverse mode (with a maximum rate of V_{SERCA}) (14) and RyR channels (J_{RyR}). The myoplasmic compartment is also in communication with the extracellular space via sarcolemmal flux (J_{sl}) that features a simplified model for Na^+-Ca^{2+} exchange (NCX) and Ca^{2+} entry via a leak pathway (assuming extracellular $[Ca^{2+}]_e$=1mM) (38).

The mathematical characterization of RyR channels is simplified to the minimum that is sufficient to encode the properties (7-10) of

- activation and inactivation by myoplasmic $[Ca^{2+}]$,
- threshold opening with high gain,
- modulation by SR $[Ca^{2+}]$.

To represent these features mathematically, RyRs were modeled as ‘release gates’, sensitive to myoplasmic and SR $[Ca^{2+}]$ (7). The simplified mathematics describe schematic population behavior of RyRs, rather than a Markovian channel representation of RyR channel clusters. Ca^{2+} flux across RyR ‘release gates’ is given by the product of their fractional activation and a permeability constant (k_{RyR}). Fractional activation is given by the difference in ‘occupancy’ of a fast, activation gate (S_α) and a slow, inactivation gate (S_β). By setting faster Ca^{2+} binding kinetics to S_α, the model encodes for time-dependent SR Ca^{2+} release: activation followed by inactivation, as proposed originally in (48). Occupancy of these two gates is described by Ca^{2+} dissociation constants K_α and K_β. The fast gate is assumed to be in equilibrium with myoplasmic Ca^{2+} whereas binding to the slow gate follows first order kinetics with on and off rate-constants k_β^+ and k_β^-, respectively.

Incorporation of the inactivation gate S_β is necessary to account for threshold. Threshold is encoded by ensuring that, below a certain rise in myoplasmic $[Ca^{2+}]$, S_β occupancy exceeds S_α occupancy, i.e. $K_\alpha > K_\beta$ at steady-state. For comparison, if $K_\alpha = K_\beta$, any rise in myoplasmic $[Ca^{2+}]$ will trigger opening and, if $K_\alpha < K_\beta$, RyR channels will open spontaneously. In other words, threshold is determined by the difference between K_α and K_β under resting conditions.

It is well-established that SR content affects Ca^{2+} wave threshold. A Ca^{2+} ‘overloaded’ SR is more prone to firing Ca^{2+} waves (40). At present, there is good experimental evidence to suggest that calsequestrin modulates RyR opening probability (8, 9). To account for RyR modulation by SR Ca^{2+} content in the model, k_β^+ is set to be linearly-dependent on calsequestrin concentration (14, 38). By implementing this, K_β and hence Ca^{2+} wave threshold become dependent on SR $[Ca^{2+}]$.

The system of equations for the model is constructed to describe a vector u for the following species:

1. free myoplasmic [Ca^{2+}],
2. Ca^{2+}-bound myoplasmic buffer,
3. unbound myoplasmic buffer,
4. free SR [Ca^{2+}],
5. Ca^{2+}-bound calsequestrin,
6. unbound calsequestrin,
7. Ca^{2+}-occupancy of (fast, activating) site S_α,
8. Ca^{2+}-occupancy of (slow, inactivating) site S_β.

The model equations are as follows:

$$\frac{\partial u_1}{\partial t} = D_1 \cdot \frac{\partial^2 u_1}{\partial x^2} - J_{Mbuf} + \frac{J_{sl} + J_{RyR} - J_{SERCA}}{v_m}$$
$$\frac{\partial u_2}{\partial t} = D_2 \cdot \frac{\partial^2 u_2}{\partial x^2} - J_{Mbuf}$$
$$\frac{\partial u_3}{\partial t} = D_3 \cdot \frac{\partial^2 u_3}{\partial x^2} + J_{Mbuf}$$
$$\frac{\partial u_4}{\partial t} = D_4 \cdot \frac{\partial^2 u_4}{\partial x^2} - J_{SRbuf} + \frac{J_{SERCA} - J_{RyR}}{v_{SR}}$$
$$\frac{\partial u_5}{\partial t} = D_5 \cdot \frac{\partial^2 u_5}{\partial x^2} - J_{SRbuf}$$
$$\frac{\partial u_6}{\partial t} = D_6 \cdot \frac{\partial^2 u_6}{\partial x^2} + J_{SRbuf}$$
$$u_7 = \frac{u_1}{u_1 + K_\alpha}$$
$$\frac{\partial u_8}{\partial t} = k_\beta^+ \cdot u_6 \cdot u_1 \cdot (1 - u_8) - K_\beta^- \cdot u_8$$

where

$$J_{Mbuf} = k_M \cdot (u_1 \cdot u_3 - K_M \cdot u_2)$$
$$J_{SRbuf} = k_{SR} \cdot (u_4 \cdot u_6 - K_{SR} \cdot u_5)$$
$$J_{RyR} = R(u_7, u_8) \cdot (u_4 - u_1)$$
$$J_{SERCA} = \frac{V_{SERCA} \cdot (u_1^2 - (u_4/\delta)^2)}{K_{SERCA}^2 + u_1^2 + (u_4/\delta)^2}$$
$$J_{sl} = k_{sl} \cdot \left(\left[Ca^{2+} \right]_e - u_1 \right) - \frac{V_{NCX} \cdot u_1}{K_{NCX} + u_1}$$

The gating of RyR channels follows the condition:

$$R = \begin{cases} k_{RyR} \cdot (u_7 - u_8) + k_{leak} & \text{if} \quad (u_7 - u_8) > 0, \\ k_{leak} & \text{otherwise} \end{cases}$$

Recent measurements of the SR leak-load relationship (49) suggest that the rate-constant for background SR Ca^{2+} leak, k_{leak}, is not constant but varies with SR [Ca^{2+}]. To implement this in the model, k_{leak} was set to vary with total SR [Ca^{2+}] raised to 1.7th power, and scaled to a level that balances SERCA flux to attain the desired steady-state SR [Ca^{2+}] load (0.063 s^{-1} for SR free [Ca^{2+}]=500μM; (49)). Parameterization of SERCA flux was based on (38). Unless stated otherwise, resting myoplasmic and SR free [Ca^{2+}] were set to 0.1μM and 500μM (6, 14, 38). The initial conditions vector is,

$$\begin{bmatrix} 0.1 & \frac{0.1 \cdot C_{mbuf}}{0.1+K_{mbuf}} & \frac{K_{mbuf} \cdot C_{mbuf}}{0.1+K_{mbuf}} & \cdots \\ 500 & \frac{500 \cdot C_{SRbuf}}{500+K_{SRbuf}} & \frac{K_{SRbuf} \cdot C_{SRbuf}}{500+K_{SRbuf}} & \cdots \\ \frac{0.1}{0.1+K_{\alpha}} & \frac{0.1}{0.1+K_{\beta}} & & \end{bmatrix}$$

The six solutes modeled are assigned diffusion coefficients D_1 to D_6 ($D_2=D_3$, $D_5=D_6$) which determine 'effective' Ca^{2+} mobility:

$$D_{Meff} = \frac{D_1 + \frac{D_2 \cdot C_{Mbuf} \cdot K_{Mbuf}}{(K_{Mbuf}+[Ca^{2+}])^2}}{1 + \frac{C_{Mbuf} \cdot K_{Mbuf}}{(K_{Mbuf}+[Ca^{2+}])^2}} \quad \text{Eq 4}$$

$$D_{SReff} = \frac{D_4 + \frac{D_5 \cdot C_{SRbuf} \cdot K_{SRbuf}}{(K_{SRbuf}+[Ca^{2+}])^2}}{1 + \frac{C_{SRbuf} \cdot K_{SRbuf}}{(K_{SRbuf}+[Ca^{2+}])^2}} \quad \text{Eq 5}$$

Myoplasmic free Ca^{2+} mobility ($D_1=D_{Mfree}$) is estimated assuming a free Ca^{2+} mobility of $1000\mu m^2/s$ and a tortuosity that reduced mobility by a factor of 2 (20). D_2 and D_3 describe myoplasmic buffer mobility (D_{Mbuf}), which was set to a single, lumped value that yields an effective Ca^{2+} mobility (D_{Meff}) of $20\mu m^2/s$ at diastolic $[Ca^{2+}]$ (Eq 4). For a cell at diastolic myoplasmic $[Ca^{2+}]$=100nM, D_{Meff} of $20\mu m^2/s$ translates to a D_{Mbuf} $18\mu m^2/s$. Calsequestrin is assumed to be immobile, therefore $D_5=D_6=0$. Intra-SR free Ca^{2+} mobility ($D_4=D_{SRfree}$) is estimated from data for effective intra-SR Ca^{2+} mobility. At half-filled SR, D_{SReff} has been estimated to be $9\mu m^2/s$, therefore $D_{SRfree}=39\mu m^2/s$ (Eq 5). To simulate changes in myoplasmic and SR Ca^{2+} mobility, variables D_{Mbuf} and D_{SRfree} were varied independently.

Since cell width and height are considerably smaller than length, the mathematics can be reduced to a one-dimensional space. The wave model is solved over a linear space x=[0,100]μm with reflection boundaries set on either end. Table 1 lists values of constants used in the modeling.

To trigger a simulated Ca^{2+} wave, SR release was activated in a 2μm-wide region, midway along the length of the model cell. This was performed by one of three maneuvers: (i) introducing an additional SR-membrane flux term, with permeability constant k_{act} in parallel to k_{RyR} and k_{leak}, (ii) by locally elevating myoplasmic $[Ca^{2+}]$ (raising k_{sl} for 20msec) or (iii) by locally over-loading SR $[Ca^{2+}]$ (introducing a constant gain in SR free $[Ca^{2+}]$ for 20ms). Maneuvers (ii) and (iii) (but not (i)) increase, albeit temporarily, the total amount of Ca^{2+} in the cell. Unless stated otherwise, *in silico* Ca^{2+} waves were triggered by (i).

4. RESULTS

4.1. Calcium mobility in myoplasm and SR is low

Low Ca^{2+} mobility has been measured in previous studies for both myoplasm (20-22) and SR (6). Figure 2A shows an experiment from (6), illustrating low Ca^{2+} mobility in SR and myoplasm. The cell was first stabilized under conditions where sarcolemmal and SR Ca^{2+} fluxes are minimized (absence of superfusate Na^+ and Ca^{2+}, presence of CPA and tetracaine). Using a dual microperfusion apparatus (6, 19), one half of the myocyte was exposed to caffeine to open RyR channels locally (arrow 1, Figure 3Aii). This produced a

local Ca^{2+} release into the myoplasm, reported by the rise in Fluo-3 signal (F/F_0). The black trace in Figure 3Aii shows the fluorescence rise averaged in the proximal, caffeine-exposed region and the grey trace shows the fluorescence rise at the other (distal) end. Note that the spread of Ca^{2+} to the distal end was small, indicating low myoplasmic Ca^{2+} mobility. After a delay of 30s, the rest of the cell was also exposed to caffeine, releasing any Ca^{2+} that had remained within the SR. Again, the spread of Ca^{2+} along the myoplasm was small, arguing for low myoplasmic Ca^{2+} mobility. This experiment also confirms low SR Ca^{2+} mobility. The whole-cell caffeine exposure (arrow 2, Figure 3Aii) produced a large release of Ca^{2+}, peaking at a level similar to that during the first, regional caffeine exposure (arrow 1, Figure 3Aii). If SR Ca^{2+} mobility were high, the local caffeine exposure would have drained distal SR regions and reduced overall $[Ca^{2+}]$ load. Since the F/F_0 peaks indicated by the two circled arrows in Figure 3Aii were of similar magnitude, SR mobility is unlikely to be fast.

Figure 3B shows model simulations for the experimental maneuver, based on the modeling framework published and validated elsewhere (6). Panel (i) shows the simulation for the best-fitting effective myoplasmic and SR Ca^{2+} mobility of D_{Mbuf}=18 and D_{SRfree}=39$\mu m^2/s$, respectively. These are equivalent to D_{Meff} and D_{SReff} of 20$\mu m^2/s$ (at diastolic myoplasmic $[Ca^{2+}]$=100nM) and 9$\mu m^2/s$ (at half-filled SR), respectively. To confirm the goodness-of-fit, the model was run for different values for D_{Mbuf} and D_{SRfree}: (ii) 180 and 39$\mu m^2/s$, (iii) 18 and 390$\mu m^2/s$, and (iv) 180 and 390$\mu m^2/s$. By inflating D_{Mbuf} and/or D_{SRfree} by one order of magnitude, the predicted F/F_0 time-courses no longer fit the data. These and similar data confirm low D_{Meff} and D_{SReff} in myocytes.

In a second set of experiments, myocytes were exposed to high superfusate Ca^{2+} (7.5mM) to induce SR Ca^{2+} overload and elicit Ca^{2+} waves (40). Figure 4 shows an experiment in which a myocyte spontaneously fired a Ca^{2+} wave (Figure 4A). After a 1s delay, the cell was field-stimulated for 2ms to evoke a Ca^{2+} transient (Figure 4B). The Ca^{2+} wave propagated at a velocity of 89$\mu m/s$ (average for 10 cells=78±5$\mu m/s$), in agreement with previous estimates for cardiac myocytes of ~100$\mu m/s$ (35). The time-course of the Ca^{2+} wave was velocity-corrected (time-frame for F/F_0 averaging was aligned with the onset of the wave, along the region denoted by the grey bar on the left of the linescan, (44)) and compared with the time-course of the Ca^{2+} transient. The time-course of the Ca^{2+} wave was similar to that of a Ca^{2+} transient. The Ca^{2+} wave onset, peak and duration were marginally slower than the corresponding parameters for the Ca^{2+} transients. The time-to-peak for the wave was ~100ms and its half-maximal width was ~180ms. Assuming a Fluo-3 dissociation constant of 850nM (6, 50), the peak rise in fluorescence corresponds to ~1μM $[Ca^{2+}]$.

4.2. Modeling calcium waves

Ca^{2+} waves were simulated to generate an estimate for their velocity, which was then correlated with the Ca^{2+} diffusion coefficients. First, several model parameters (denoted by # in Table 1) were adjusted to obtain Ca^{2+} wave velocity and time-course similar to that measured experimentally (Figure 4). The interaction of Ca^{2+} with the S_α and S_β gates was described with dissociation constants K_α and K_β that were set to be within the experimentally-determined range of 300-700nM (38, 51). The difference between K_α and K_β determines threshold for Ca^{2+} wave initiation. Under resting conditions, release events that raise myoplasmic $[Ca^{2+}]$ locally to >200nM trigger waves (44), therefore under resting conditions ($[Ca^{2+}]_{SR}$=500μM, $[Ca^{2+}]_M$=0.1μM), K_α and K_β were set to 400nM and 300nM, respectively. The value for activated RyR permeability (k_{RyR}) was derived by best-fitting to Ca^{2+} wave velocity and the rate of myoplasmic $[Ca^{2+}]$ rise (Figure 4A, (44)). The magnitude of k_{RyR}, together with the threshold for RyR channel activation, will set the time-delay for triggering Ca^{2+} release. These parameters will therefore affect Ca^{2+} wave velocity.

The model also predicts Ca^{2+} wave propagation failure when free [Ca^{2+}] in the SR falls below 365μM, i.e. 73% of resting [Ca^{2+}]. This is in agreement with experimental data (52) that have shown Ca^{2+} wave propagation failure when total SR load falls by >25% (absence of Ca^{2+} waves for total SR [Ca^{2+}]<90μmol/ (L cytosol), assuming total [Ca^{2+}] in filled SR of 120μmol/(L cytosol)).

The model output is presented in Figure 5 in the form of linescans for myoplasmic and SR [Ca^{2+}]. SR release was triggered locally (middle 2μm-wide region) by introducing an additional, exponentially-decaying term for SR Ca^{2+} permeability k_{act} (t) in parallel to k_{RyR} and k_{leak}. The initial amplitude of k_{act} was varied to probe for the threshold for Ca^{2+} wave generation. Below the threshold, SR release produced a local event that resembled a Ca^{2+} spark in the myoplasm (Figure 5Ai) and an associated Ca^{2+} blink (local luminal depletion) in the SR (Figure 5Bi). By setting the time-constant for k_{act} to 10ms, the spark and blink recovery time-constants were 25 and 75ms, within the experimentally-determined range (26, 29, 31). Above the threshold, the model generated a Ca^{2+} wave of velocity 78μm/s in the myoplasm (Figure 5Aii) and SR (Figure 5Bii). The model predicts a [Ca^{2+}] rise in the myoplasm during the wave, accompanied by a simultaneous wave of [Ca^{2+}] depletion in the SR. The time-courses of the myoplasmic release and SR depletion waves are plotted, together with the time-courses of the simulated Ca^{2+} 'spark' and 'blink'. To compare the simulated time-course with experimental data, myoplasmic and SR [Ca^{2+}] were converted to normalized Fluo-3 and Fluo-5 fluorescence (Figure 5C), assuming dissociation constants of 850nM (6, 50) and 400μM (27), respectively. The myoplasmic Ca^{2+} time-course is in agreement with experimental data (Figure 4A). The maximum local SR [Ca^{2+}] depletion (~60%) is also in agreement with predictions based on experiments (38).

The trigger for the simulated waves in Figure 5 was RyR activation imposed by an additional term for permeability. Physiologically, RyR activation can occur as a result of a rise in myoplasmic [Ca^{2+}] or a rise in SR [Ca^{2+}]. These were implemented mathematically by introducing a constant Ca^{2+} flux in the myoplasm or SR for 20ms in a central, 2μm-wide region in the myocyte. The magnitude was set to a supra-threshold level for wave generation. The outcome of the two triggering protocols was very similar (Figure 6). This is not surprising, given that the unified model uses the same equations for both modes of triggering. It is noteworthy that the simulated wave of SR [Ca^{2+}] depletion is sharp, as determined experimentally (28, 53) and as expected from slow SR Ca^{2+} mobility (6) (but cf (27, 41)).

4.3. Modeling calcium waves at different calcium diffusion coefficients

In this set of simulations, effective Ca^{2+} mobility in myoplasm (D_{Meff}) and SR (D_{SReff}) were varied independently. This was performed by varying D_{Mbuf} between zero and 100μm^2/s (D_{Meff}=102μm^2/s) and D_{SRfree} between zero and 500μm^2/s (D_{SReff}=160μm^2/s). Ca^{2+} waves were triggered by opening RyR channels (introducing permeability k_{act}). At constant, control D_{SRfree}=39μm^2/s, increasing D_{Mbuf} (and D_{Meff}) *increased* wave velocity sub-linearly over the range studied (Figure 7A). This is expected, as increasing mobility will decrease the time-delay due to diffusion between adjacent release sites. According to the model, velocity is proportional to the square root of diffusion coefficient D_{Mbuf} (Figure 7A). This is expected from continuum models (46). In fire-diffuse-fire models with discrete release sites, velocity has been proposed to vary proportionally with diffusion coefficient (47, 54) because the rate of wave progression is limited by the diffusion delay between discrete release sites rather than the release kinetics. In the presented continuum model, the slope of the mobility-velocity relationship (Figure 7A) falls at high Ca^{2+} mobility because the time-delay incurred by the opening of RyR channels becomes a more significant limiting factor towards overall Ca^{2+} wave velocity.

At constant D_{Mbuf}=18μm^2/s, increasing D_{SRfree} *decreased* wave velocity (Figure 7B) proportionately with the square root of D_{SRfree}. At high D_{SRfree} (as proposed for the model illustrated in Figure 2C), waves propagate at a velocity much slower than measured experimentally. This observation is somewhat less intuitive than the relationship in Figure 7A. Following a local SR release event, low D_{SRfree} (hence low D_{SReff}) will protect adjacent SR regions from diffusive dissipation. This will preserve Ca^{2+} substrate for SR release and hence wave propagation. Conversely, at high D_{SReff}, a local SR release will lead to depletion of adjacent SR regions. Consequently, myoplasmic Ca^{2+} will have to travel a longer distance (i.e. longer time-delay) to the next available SR region that can support release. This phenomenon is emphasized by the modulation of S_{α}-Ca^{2+} interaction kinetics by SR [Ca^{2+}]. However, even without this additional cross-talk, the negative slope between D_{SRfree} and velocity remains qualitatively true.

Figure 7C shows the results of simulations in the form of a contour map. To summarize, the modeling predicts that increasing myoplasmic Ca^{2+} mobility and decreasing SR Ca^{2+} mobility will favor faster Ca^{2+} wave propagation.

4.4. Modeling calcium waves at different SERCA pump rates and RyR permeability

The local SR [Ca^{2+}] available for release is dependent on diffusive dissipation and also on the replenishing activity of the SR Ca^{2+} pump, SERCA. Experimental results have yielded apparently conflicting inferences on the effect of SERCA inhibitors on wave velocity (a decrease (41, 55) or an increase (40)). As highlighted by others (55), the effect of SERCA inhibitors is two-fold. On the one hand, inhibition of SERCA reduces Ca^{2+} uptake from myoplasm, and therefore permits myoplasmic Ca^{2+} to diffuse a longer distance to reach more distant release sites. This factor increases wave velocity. From this point of view, SERCA behaves like a 'Ca^{2+} buffer' (indeed, increasing the dose of the Ca^{2+} buffer EGTA decreases wave velocity (56)). On the other hand, inhibition of SERCA will also reduce SR load and reduce the substrate for release. Furthermore, since SR Ca^{2+} modulates RyR channels (37, 38), a fall in local SR load will reduce the likelihood of RyR channel opening. These factors will tend to reduce Ca^{2+} wave velocity.

The model was configured with V_{SERCA} manipulated to between 0.2- and 2-fold of control activity, while D_{Mbuf} and D_{SRfree} were maintained at 18 and 39μm^2/s. A Ca^{2+} wave was triggered (activating permeability k_{act}) immediately after manipulating V_{SERCA} or after a delay of 0.3, 0.6, 1 or 1.5s. The output of the model is shown in Figure 8Ai. If the Ca^{2+} wave is triggered early (<0.4s) after SERCA manipulation, the model predicts a negative relationship between V_{SERCA} and velocity. Over this short time-delay, the SR Ca^{2+} load will not change significantly. However, the altered activity of SERCA will have an immediate effect on the spatial spread of myoplasmic Ca^{2+}. Under these conditions, the higher the SERCA activity, the smaller the spatial spread of myoplasmic Ca^{2+} and hence the slower the wave (40), as expected from the EGTA-like 'buffer' effect of SERCA (56). If the Ca^{2+} wave is triggered after a longer delay (>0.4s) following SERCA inhibition, the SR load has had enough time to change, particularly when the starting SR [Ca^{2+}] is high (the SR leak-load relationship is exponential, (49)). Under these conditions, the spatial range of myoplasmic Ca^{2+} diffusion will be secondary to the effect of SR load on RyR channels: the lower the SR load, the slower the wave velocity. Our model therefore highlights the complexity of factors that affect Ca^{2+} wave velocity. Interpretation of experimental data must be made carefully in order to produce a unified hypothesis for the mechanism of Ca^{2+} waves. The star symbol indicates mean, normalized Ca^{2+} wave velocity, measured experimentally after 1s of inhibiting SERCA to a level that slows Ca^{2+} recovery 2.4-fold (41) (equivalent to 70% reduction in V_{SERCA}). The data are in good agreement with the mathematical prediction, i.e. SERCA inhibition slows wave velocity. Moreover, the slowing can occur without a major

change in wave amplitude, as the smaller Ca^{2+} release (due to reduced SR load) is balanced by the slower SERCA kinetics that allow myoplasmic $[Ca^{2+}]$ to stay elevated for longer.

To illustrate the importance of SR load on Ca^{2+} wave velocity, the model was used to plot Ca^{2+} wave velocity against SR $[Ca^{2+}]$ (measured at 5μm from the trigger site). Reducing SERCA activity reduces SR free $[Ca^{2+}]$ and increases k_{β}^{+} which, in turn, elevates the threshold for Ca^{2+} release and reduces wave velocity. The experimental result (41) plotted in Figure 8Ai (green star) has been re-plotted in Figure 8Aii, again showing agreement with the predicted slowing of wave velocity. This prediction is also in agreement with recent experimental data (57) showing that a reduction in SERCA expression (42% reduction in rate) reduces Ca^{2+} wave velocity (red triangle, Figure 8Aii).

SR Ca^{2+} is released into the myoplasm through both a triggered and a leak pathway. There is good evidence to suggest that both pathways are mediated by RyR channels, but it is possible that the SR background leak occurs, at least partly, via 'rogue' RyR channels located outside couplons (58). In our model, Ca^{2+} fluxes are described by constants k_{RyR} and k_{leak}, respectively, and can be varied independently. Experimentally, however, pharmacological modulation of RyR channels with drugs such as tetracaine (an inhibitor) or caffeine (an activator) may affect both k_{RyR} and k_{leak}. Perhaps not surprisingly, the effect of tetracaine on Ca^{2+} wave velocity is complex. In some studies, tetracaine has been reported to slow wave velocity (59). Other studies have proposed a dose-dependence (60), such that lower tetracaine doses (<0.5mM) accelerated Ca^{2+} waves and higher doses (>0.5mM) tended to slow propagation.

In an attempt to reconcile the above findings with the proposed model for Ca^{2+} wave propagation, we performed two simulations. In the first, k_{RyR} was varied between 20% and 200% of its control rate while D_{Mbuf} and D_{SRfree} were fixed at 18 and 39$\mu m^2/s$. This computational maneuver altered the population permeability of activated RyR channels. The black curve in Figure 8Bi shows the output of this simulation. Ca^{2+} wave velocity increased with increasing activated RyR permeability. This is predicted intuitively, as a faster development of RyR conductance will lead to faster Ca^{2+} release, which in turn will have a knock-on effect in reducing the time-delay associated with triggering the adjacent SR release event. Such a positive-slope relationship has been obtained experimentally with low doses of caffeine which increases wave velocity (39, 61) or, under certain conditions, with tetracaine which decrease wave velocity (59, 60). By increasing the rate of Ca^{2+} release, increasing k_{RyR} will also increase overall Ca^{2+} wave amplitude. The model was used to plot Ca^{2+} wave velocity versus peak myoplasmic $[Ca^{2+}]$ during a Ca^{2+} wave measured at 5μm from the trigger site (Figure 8Bii). The positive velocity-amplitude relationship is backed by experimental data (39, 59). Conversely, when k_{RyR} is reduced below 45% of its control value, Ca^{2+} waves fail to propagate (black star, Figure 8Bi). Experimentally, tetracaine doses in excess of 0.75mM have been shown to abolish waves within 1 min of application (60). This is equivalent to a 58% reduction in k_{RyR} (60), in approximate agreement with the model prediction.

In a second set of simulations, k_{leak} was varied instead of k_{RyR}. The model equations were first allowed to attain steady-state at the new value for k_{leak}. This was necessary in order to re-adjust diastolic SR $[Ca^{2+}]$, which is set by the balance between background SR leak and SERCA activity. The output of this simulation is shown as the red curve in Figure 8Bi. This relationship is strikingly different from the previous simulation. As k_{leak} decreases, Ca^{2+} wave velocity *increases*. This relationship has been reported at low doses of tetracaine (60). The dominant factor in shaping the difference between the two curves in Figure 8Bi is most likely to be SR $[Ca^{2+}]$ load. Alterations to k_{leak}, unlike k_{RyR}, change diastolic SR $[Ca^{2+}]$. Since SR $[Ca^{2+}]$ modulates RyR sensitivity to myoplasmic $[Ca^{2+}]$, k_{leak} will affect the

threshold for triggering SR Ca^{2+} release. High SR Ca^{2+} leak will lower SR [Ca^{2+}] which, in turn, will elevate the threshold for Ca^{2+} release by raising k_{β}^{+}. This will favor slower Ca^{2+} wave propagation, as predicted by the model. If k_{leak} is raised >1.8-fold, free [Ca^{2+}] in the SR drops to <365μM and Ca^{2+} waves fail to propagate (red star, Figure 8Bi), in agreement with experimental data (52).

In a third set of simulations, k_{RyR} and k_{leak} were manipulated simultaneously (Figure 8Bi, green curve) and the system was allowed to attain a new steady-state at the new value for k_{leak}. Under steady-state conditions, adding RyR inhibitors or openers are likely to produce parallel changes in both k_{RyR} and k_{leak}. The predicted relationship is positive and approximately linear, indicating that the rate of Ca^{2+} rise (k_{RyR}) is the major determinant of Ca^{2+} wave velocity.

The effect of k_{RyR}+k_{leak} on Ca^{2+} wave velocity was studied further at different values of D_{Mbuf} and D_{SRfree}. The purpose of this final set of simulations was to identify the combination of RyR permeability and Ca^{2+} diffusion in myoplasm and SR at which Ca^{2+} wave velocity is 78μm/s. The output of the model is presented in Figure 9A. This figure can be used to identify the set of conditions that is compatible with normal Ca^{2+} wave velocity. If, for example, D_{SReff} were higher than 9μm^2/s, then a higher D_{Meff} and/or higher k_{RyR}+k_{leak} would be necessary to predict a wave velocity of 78μm/s. Specifically, if D_{SReff} were 60μm^2/s (as measured in (27)) and D_{Meff} were 20μm^2/s, wave velocity of 78μm/s would require k_{RyR} and k_{leak} to be 1.6-fold higher, i.e. the rising slope of the myoplasmic Ca^{2+} wave would be steeper (due to k_{RyR}) and SR [Ca^{2+}] load would be smaller (due to k_{leak}). Conversely, if present estimates for D_{Meff} have been under-estimated, D_{SReff} will need to be higher and/or k_{RyR} lower to obtain the desired 78μm/s velocity. It is noteworthy that the model predicts the experimentally measured wave velocity using an experimentally-derived wave rising-slope and independently-derived diffusion coefficients.

As a final point, we investigated the temporal relationship between myoplasmic and SR [Ca^{2+}] in an attempt to identify whether a myoplasmic or SR wavefront drives the Ca^{2+} wave. This underpins the difference between classical (Figure 2B) and the more recent (Figure 2C, (41)) proposals for the mechanism for Ca^{2+} wave propagation. The Ca^{2+} wave simulated in Figure 5 was analyzed first. This wave was triggered under conditions of control Ca^{2+} mobility and RyR permeability (D_{Mbuf}=18μm^2/s; D_{SRfree}=39μm^2/s; wave velocity=78μm/s). Myoplasmic and SR [Ca^{2+}], at different distances from the trigger site, were plotted as hysteresis loops, shown in Figure 9Bi. The loops were clockwise, indicating that the rise in myoplasmic [Ca^{2+}] occurred *before* the fall in SR [Ca^{2+}], i.e. a component of the myoplasmic [Ca^{2+}] rise is due to diffusion from elsewhere within the myoplasm. Also, the slope of the loops over the rising phase of the Ca^{2+} wave was consistently negative, indicating that a rise in SR [Ca^{2+}] never traveled ahead of the rise in myoplasmic [Ca^{2+}]. Our second simulation attempted to address an alternative proposal for Ca^{2+} wave propagation, in which fast intra-SR Ca^{2+} diffusion produces a wavefront of sensitized RyR channels ahead of the myoplasmic [Ca^{2+}] wavefront (Figure 2C, (41)). The wave was simulated under conditions of fast SR mobility (D_{SRfree}=195μm^2/s giving D_{SReff}=60μm^2/s for half-filled SR) and appropriately elevated k_{RyR} to obtain 78μm/s wave velocity (see Figure 9A). The hysteresis loops for this simulation are shown in Figure 9Bii. Again, the hysteresis loops were clockwise. Thus, the rising phase of the myoplasmic Ca^{2+} wave was *not* preceded by a rise of SR [Ca^{2+}], excluding the possibility that a wavefront of RyR sensitization travels ahead of the myoplasmic [Ca^{2+}] wavefront. These loops, generated under two different simulation conditions, strengthen the hypothesis that Ca^{2+} waves are driven by a myoplasmic Ca^{2+} wavefront (Figure 9C) that is not preceded by elevated (RyR-sensitizing) SR [Ca^{2+}].

5. DISCUSSION

5.1. Role of Ca^{2+} mobility and SR Ca^{2+}-load in wave propagation

Ca^{2+} waves play a significant role in cardiac myocyte physiology, particularly under pathological conditions such as Ca^{2+} overload. It has been argued that Ca^{2+} waves may serve to eliminate SR overload by stimulating Na^{+}-Ca^{2+} exchange to extrude excess Ca^{2+} although, paradoxically, the very same process underlies their arrhythmogenic properties (62). Experimental studies of Ca^{2+} waves have helped to refine our understanding of Ca^{2+} signaling mechanisms (35, 36). Analyses of Ca^{2+} waves have also offered novel approaches to calibrating dyes (50) and for measuring SERCA kinetics (44).

The benefits of our modeling are four-fold. *Firstly*, the model offers a simple mathematical framework to accompany experimental investigations into the mechanism of Ca^{2+} waves. A key output of the model is wave velocity which is a readily-measurable parameter. The model can be used to test if a particular cellular parameter (such as a Ca^{2+} flux rate or diffusion coefficient) is consistent with measured velocity. For instance, Figure 9A can be used as a look-up table to derive the missing parameter if the other two are known (among Ca^{2+} diffusion in SR, Ca^{2+} diffusion in myoplasm, RyR permeability). Although many combinations of D_{SReff} and D_{Meff} predict a wave velocity of 78μm/s, only a narrow range also satisfies the criterion for RyR permeability which can be estimated experimentally from the time-course of the Ca^{2+} wave.

Secondly, the model illustrates the importance of ionic mobility in determining Ca^{2+} wave velocity. Our simulations confirm the well-established importance of myoplasmic Ca^{2+} diffusion in setting wave velocity (Figure 7A). In addition, the simulations show that Ca^{2+} wave velocity is very sensitive to the Ca^{2+} diffusion coefficient in the SR (Figure 7B). This finding is both novel and important, as SR Ca^{2+} mobility has only recently been measured (6, 27). Many previous models have made assumptions of zero SR Ca^{2+} mobility (e.g. (43, 44)) or finite mobility (e.g. (46)) with no strong experimental backing.

Thirdly, the model offers a unifying framework which can explain seemingly conflicting observations. One illustration of this has been presented in Figure 8A for the effects of SERCA activity on wave velocity. Experiments have determined that inhibition of SERCA either decreases (41, 55) or increases (40) wave velocity. The model can predict both responses, depending on the circumstances. Another example of the usefulness of the model is in the interpretation of experiments in which RyR channels are modulated pharmacologically. In Figure 8B, we have shown that such modulation can either increase or decrease wave velocity. This is because there are potentially two effects of RyR-targeting drugs (such as tetracaine or caffeine). One will be a modulation of the background SR Ca^{2+} leak, and the other will be a modulation of the rate of Ca^{2+} release through triggered RyR channels during the rising phase of a Ca^{2+} wave. The onset of the latter effect will be immediate. The former effect will change wave velocity by adjusting SR [Ca^{2+}] load. This, however, will take longer to develop. If the background leak is affected, the dominant influence on wave velocity will be via SR [Ca^{2+}] load, and thus the sensitization of RyR channels to myoplasmic [Ca^{2+}]. Otherwise, if modulation of triggered RyR channels prevails, wave velocity will be affected by the myoplasmic [Ca^{2+}] rise-time, i.e. the time-delay to threshold. Such a mechanism may explain the positive relationship between caffeine dose and Ca^{2+} wave velocity (61) and the slowing effect that tetracaine has on Ca^{2+} waves (59, 60) (albeit at higher doses in (60)). It is possible that inhibition of background leak requires a more sustained but lower tetracaine dose, explaining why, in one study, low doses of the drug (<0.5mM) accelerated Ca^{2+} waves (60).

Fourthly, the model can help in testing for the feasibility of proposed hypotheses for Ca^{2+} wave propagation. For instance, an earlier finding that SERCA inhibition leads to wave slowing has spawned an alternative hypothesis for the mechanism of Ca^{2+} waves (41), in which a wave of elevated SR [Ca^{2+}] (supported, for example, by advance SERCA activity) travels ahead of the myoplasmic [Ca^{2+}] wavefront. This hypothesis (Figure 2C) would necessitate fast SR Ca^{2+} mobility (D_{SReff}). Our model can predict a fall in wave velocity when SERCA is down-regulated, without having to assume a high D_{SReff}. Indeed even at high D_{SReff}, simulated Ca^{2+} waves follow the classical model of propagation illustrated in Figure 2B, i.e. myoplasmic-driven Ca^{2+} wave propagation without a preceding wavefront of elevated SR [Ca^{2+}]. A plot of myoplasmic [Ca^{2+}] versus SR [Ca^{2+}] during a simulated Ca^{2+} wave (Figure 9B) reveals a clock-wise hysteresis, indicating that the rise in myoplasmic Ca^{2+} occurs before a fall in SR [Ca^{2+}]. None of the simulations performed using our model predicted a rise in SR [Ca^{2+}] that would drive wave propagation. Moreover, the simulated SR [Ca^{2+}] wavefront is sharp and biphasic (Figures 5, 6) in agreement with experimental evidence obtained with intra-SR Ca^{2+} dyes (28, 53), an observation that supports the presence of low SR Ca^{2+} mobility. Although high SR Ca^{2+} mobility would favor faster spread of an intra-SR Ca^{2+} overload, once the SR Ca^{2+} wave encounters sensitized RyR channels, SR Ca^{2+} is released and the intra-SR diffusion gradient for wavefront progression will be abolished, or even reversed.

5.2. Model limitations

The present work presents a simplified, continuum, common-pool model for a Ca^{2+} wave (for criticism of common-pool models, see (63); for criticism of continuum models, see (47)). The model was deliberately simple to reduce the number of uncertain or unresolved variables and to reduce computational time to the order of tens of seconds on a 2GHz processor. More sophisticated models should include a fuzzy space between SR and myoplasm (e.g. (38)). Although the introduction of a third compartment is mathematically justifiable, it would be difficult to parameterize fully, e.g. with respect to buffering and Ca^{2+} mobility. The model does not encode for a precise geometrical relationship between RyR channels and SERCA and does not distinguish between junctional and network SR. At the scale of this fine detail, a continuum approximation is valid given that diffusion delays between junctional and network SR (64) and between RyR and SERCA (65) are likely to be small. As discussed earlier, however, the continuum approximation will generate a nonlinear dependence of wave velocity on diffusion coefficient (Figure 7A) (46, 66). In fire-diffuse-fire models with discrete release sites, wave velocity has been proposed to vary proportionally with diffusion coefficient (47, 54). In cardiac myocytes, the 1.8μm spacing between RyR release sites (67) is sufficiently large to support a discrete fire-diffuse-fire model. Moreover, some studies have hinted at discrete release sites during wave propagation (56). The relationship predicted by our model may under-estimate wave velocity at very high mobility. On the other hand, measurements of the temperature dependence of Ca^{2+} wave velocity (66) suggest an activation energy that is 28% higher than the activation energy predicted for Ca^{2+} diffusion. This implies a diffusion-independent step affects Ca^{2+} wave velocity. This may suggest that the mobility-velocity relationship may be sub-linear for high Ca^{2+} diffusion coefficients. A rigorous validation of the mobility-velocity relationship must await a full experimental characterization of the Ca^{2+} diffusion coefficient-dependence of Ca^{2+} wave velocity.

Finally, the RyR gating model used in the present Ca^{2+} wave model is simple and not intended to present a fully mechanistic Markovian representation for the binding and gating events in the RyR (cf (68)). It does, however, comply with the desired properties of threshold, activation by myoplasmic Ca^{2+} and subsequent inactivation, and modulation by SR Ca^{2+}.

5.3. Conclusions

We have constructed a mathematical framework for simulating myoplasmic and SR Ca^{2+} waves. By simplifying the mathematical representation for RyR channel gating and by reducing the *in silico* cell to two 1-D compartments, it was possible to parameterize the equation variables using experimental data obtained for rat myocytes in the present work (Figure 4) or from previous studies (e.g. (6, 14, 38)). Using experimentally-derived effective myoplasmic and SR Ca^{2+} mobility values of 20 and 9μm^2/s (Figure 3), the model predicts Ca^{2+} wave velocity of 78μm/s, in agreement with independent experimental observations. A wave velocity of 78μm/s is not given uniquely by the measured Ca^{2+} mobility (Figure 9B). However, other combinations would significantly alter the time-course of the Ca^{2+} wave, which would no longer confirm with experimental data. A supra-threshold rise in myoplasmic [Ca^{2+}], SR [Ca^{2+}] (SR overload), or both, give indistinguishable Ca^{2+} wave characteristics away from the trigger site (Figure 6). The model also explains seemingly conflicting data obtained by pharmacological manipulation of the SERCA pump or of RyR channels (40, 41, 55, 59-61). It emphasizes the importance of SR [Ca^{2+}] load, which cross-talks with the myoplasmic-facing activating sites on RyR channels (Figure 8) (8, 9). Our model also tests the feasibility of opposing hypotheses for the mechanism of wave propagation (Figure 2B vs C). We show that high SR Ca^{2+} mobility favors slow wave propagation (Figure 6). The spread of an intra-SR [Ca^{2+}] overload cannot drive a Ca^{2+} wave since this would be self-limiting. Diffusive progression of an intra-SR [Ca^{2+}] wave will be terminated the instant that RyR channels open, thereby abolishing, or even reversing, the intra-SR driving force for the SR [Ca^{2+}] wavefront. Our modeling indicates a myoplasmic rather than an SR-driven model of Ca^{2+} wave propagation (Figure 9C), a conclusion supported by recent proposals for slow SR Ca^{2+} mobility (6, 31).

Acknowledgments

We wish to thank the Wellcome Trust Human Physiome Project and British Heart Foundation (to RDVJ), Royal Society and Medical Research Council (to PS), and the National Institutes of Health (grant R37HL042873) and the Nora Eccles Treadwell Foundation (to KWS) for support.

7. REFERENCES

1. Berridge MJ, Lipp P, Bootman MD. The versatility and universality of calcium signalling. Nat Rev Mol Cell Biol. 2000; 1:11–21. [PubMed: 11413485]
2. Orchard CH, Eisner DA, Allen DG. Oscillations of intracellular Ca^{2+} in mammalian cardiac muscle. Nature. 1983; 304:735–8. [PubMed: 6888540]
3. Wier WG, Cannell MB, Berlin JR, Marban E, Lederer WJ. Cellular and subcellular heterogeneity of Ca^{2+}_i in single heart cells revealed by fura-2. Science. 1987; 235:325–8. [PubMed: 3798114]
4. Berlin JR, Cannell MB, Lederer WJ. Cellular origins of the transient inward current in cardiac myocytes. Role of fluctuations and waves of elevated intracellular calcium. Circ Res. 1989; 65:115–26. [PubMed: 2736729]
5. Bers DM. Calcium cycling and signaling in cardiac myocytes. Annu Rev Physiol. 2008; 70:23–49. [PubMed: 17988210]
6. Swietach P, Spitzer KW, Vaughan-Jones RD. Ca^{2+}-mobility in the sarcoplasmic reticulum of ventricular myocytes is low. Biophys J. 2008; 95:1412–27. [PubMed: 18390622]
7. Laver DR. Ca^{2+} stores regulate ryanodine receptor Ca^{2+} release channels via luminal and cytosolic Ca^{2+} sites. Biophys J. 2007; 92:3541–55. [PubMed: 17351009]
8. Shannon TR. Linking calsequestrin to lumenal control of SR Ca^{2+} release. Circ Res. 2007; 101:539–41. [PubMed: 17872471]
9. Chopra N, Kannankeril PJ, Yang T, Hlaing T, Holinstat I, Ettensohn K, Pfeifer K, Akin B, Jones LR, Franzini-Armstrong C, Knollmann BC. Modest reductions of cardiac calsequestrin increase

sarcoplasmic reticulum Ca^{2+} leak independent of luminal Ca^{2+} and trigger ventricular arrhythmias in mice. Circ Res. 2007; 101:617–26. [PubMed: 17656677]

10. Fabiato A. Calcium-induced release of calcium from the cardiac sarcoplasmic reticulum. Am J Physiol. 1983; 245:C1–14. [PubMed: 6346892]
11. Venetucci LA, Trafford AW, Eisner DA. Increasing ryanodine receptor open probability alone does not produce arrhythmogenic calcium waves: threshold sarcoplasmic reticulum calcium content is required. Circ Res. 2007; 100:105–11. [PubMed: 17110597]
12. Bers, DM. Ca^{2+} sources and sinks. In: Bers, DM., editor. Excitation-contraction coupling and cardiac contractile force. Kluwer Academic; Dordrecht, The Netherlands: 2001.
13. Trafford AW, Diaz ME, Eisner DA. A novel, rapid and reversible method to measure Ca^{2+} buffering and time-course of total sarcoplasmic reticulum Ca^{2+} content in cardiac ventricular myocytes. Pflugers Arch. 1999; 437:501–3. [PubMed: 9914410]
14. Shannon TR, Ginsburg KS, Bers DM. Reverse mode of the sarcoplasmic reticulum calcium pump and load-dependent cytosolic calcium decline in voltage-clamped cardiac ventricular myocytes. Biophys J. 2000; 78:322–33. [PubMed: 10620296]
15. Hove-Madsen L, Bers DM. Passive Ca^{2+} buffering and SR Ca^{2+} uptake in permeabilized rabbit ventricular myocytes. Am J Physiol. 1993; 264:C677–86. [PubMed: 7681625]
16. Berlin JR, Bassani JW, Bers DM. Intrinsic cytosolic calcium buffering properties of single rat cardiac myocytes. Biophys J. 1994; 67:1775–87. [PubMed: 7819510]
17. Wagner J, Keizer J. Effects of rapid buffers on Ca^{2+} diffusion and Ca^{2+} oscillations. Biophys J. 1994; 67:447–56. [PubMed: 7919018]
18. Vanysek, P. Ionic conductivity and diffusion at infinite dilution. In: Linde, DR., editor. CRC Handbook of Chemistry and Physics, Thermochemistry, Electrochemistry and Kinetics. CRC; London: 1999.
19. Swietach P, Leem CH, Spitzer KW, Vaughan-Jones RD. Experimental generation and computational modeling of intracellular pH gradients in cardiac myocytes. Biophys J. 2005; 88:3018–37. [PubMed: 15653720]
20. Kushmerick MJ, Podolsky RJ. Ionic mobility in muscle cells. Science. 1969; 166:1297–8. [PubMed: 5350329]
21. Baylor SM, Hollingworth S. Model of sarcomeric Ca^{2+} movements, including ATP Ca^{2+} binding and diffusion, during activation of frog skeletal muscle. J Gen Physiol. 1998; 112:297–316. [PubMed: 9725890]
22. Cordeiro JM, Spitzer KW, Giles WR, Ershler PE, Cannell MB, Bridge JH. Location of the initiation site of calcium transients and sparks in rabbit heart Purkinje cells. J Physiol. 2001; 531:301–14. [PubMed: 11310434]
23. Allbritton NL, Meyer T, Stryer L. Range of messenger action of calcium ion and inositol 1,4,5-trisphosphate. Science. 1992; 258:1812–5. [PubMed: 1465619]
24. Gabso M, Neher E, Spira ME. Low mobility of the Ca^{2+} buffers in axons of cultured Aplysia neurons. Neuron. 1997; 18:473–81. [PubMed: 9115740]
25. Smith G, MacQuaide N. Cytoplasmic versus intra-SR: the battle of the Ca^{2+} diffusion coefficients in cardiac muscle. Biophys J. 2008; 95:1005–6. [PubMed: 18469088]
26. Cheng H, Lederer WJ, Cannell MB. Calcium sparks: elementary events underlying excitation-contraction coupling in heart muscle. Science. 1993; 262:740–4. [PubMed: 8235594]
27. Wu X, Bers DM. Sarcoplasmic reticulum and nuclear envelope are one highly interconnected Ca^{2+} store throughout cardiac myocyte. Circ Res. 2006; 99:283–91. [PubMed: 16794184]
28. Stern MD, Cheng H. Putting out the fire: what terminates calcium-induced calcium release in cardiac muscle? Cell Calcium. 2004; 35:591–601. [PubMed: 15110149]
29. Brochet DX, Yang D, Di Maio A, Lederer WJ, Franzini-Armstrong C, Cheng H. Ca^{2+} blinks: rapid nanoscopic store calcium signaling. Proc Natl Acad Sci U S A. 2005; 102:3099–104. [PubMed: 15710901]
30. Kubalova Z, Terentyev D, Viatchenko-Karpinski S, Nishijima Y, Gyorke I, Terentyeva R, da Cunha DN, Sridhar A, Feldman DS, Hamlin RL, Carnes CA, Gyorke S. Abnormal intrastore calcium signaling in chronic heart failure. Proc Natl Acad Sci U S A. 2005; 102:14104–9. [PubMed: 16172392]

31. Zima AV, Picht E, Bers DM, Blatter LA. Termination of cardiac Ca^{2+} sparks: role of intra-SR Ca^{2+}, release flux, and intra-SR Ca2+ diffusion. Circ Res. 2008; 103:e105–15. [PubMed: 18787194]
32. Fabiato A, Fabiato F. Excitation-contraction coupling of isolated cardiac fibers with disrupted or closed sarcolemmas. Calcium-dependent cyclic and tonic contractions. Circ Res. 1972; 31:293–307. [PubMed: 4341466]
33. Kort AA, Capogrossi MC, Lakatta EG. Frequency, amplitude, and propagation velocity of spontaneous Ca^{2+}-dependent contractile waves in intact adult rat cardiac muscle and isolated myocytes. Circ Res. 1985; 57:844–55. [PubMed: 4064258]
34. Cheng H, Lederer MR, Lederer WJ, Cannell MB. Calcium sparks and Ca^{2+}_i waves in cardiac myocytes. Am J Physiol. 1996; 270:C148–59. [PubMed: 8772440]
35. Jaffe LF. The path of calcium in cytosolic calcium oscillations: a unifying hypothesis. Proc Natl Acad Sci U S A. 1991; 88:9883–7. [PubMed: 1946414]
36. Sneyd J, Keizer J, Sanderson MJ. Mechanisms of calcium oscillations and waves: a quantitative analysis. Faseb J. 1995; 9:1463–72. [PubMed: 7589988]
37. Gyorke I, Gyorke S. Regulation of the cardiac ryanodine receptor channel by luminal Ca^{2+} involves luminal Ca^{2+} sensing sites. Biophys J. 1998; 75:2801–10. [PubMed: 9826602]
38. Snyder SM, Palmer BM, Moore RL. A mathematical model of cardiocyte Ca^{2+} dynamics with a novel representation of sarcoplasmic reticular Ca^{2+} control. Biophys J. 2000; 79:94–115. [PubMed: 10866940]
39. Trafford AW, Lipp P, O'Neill SC, Niggli E, Eisner DA. Propagating calcium waves initiated by local caffeine application in rat ventricular myocytes. J Physiol. 1995; 489(Pt 2):319–26. [PubMed: 8847628]
40. Lukyanenko V, Subramanian S, Gyorke I, Wiesner TF, Gyorke S. The role of luminal Ca^{2+} in the generation of Ca^{2+} waves in rat ventricular myocytes. J Physiol. 1999; 518(Pt 1):173–86. [PubMed: 10373699]
41. Keller M, Kao JP, Egger M, Niggli E. Calcium waves driven by "sensitization" wave-fronts. Cardiovasc Res. 2007; 74:39–45. [PubMed: 17336953]
42. Hodgkin AL, Rushton WA. The electrical constants of crustacean nerve fibre. Proc R Soc B. 1946; 133:444–7.
43. Coombes S, Hinch R, Timofeeva Y. Receptors, sparks and waves in a fire-diffuse-fire framework for calcium release. Prog Biophys Mol Biol. 2004; 85:197–216. [PubMed: 15142744]
44. MacQuaide N, Dempster J, Smith GL. Measurement and modeling of Ca^{2+} waves in isolated rabbit ventricular cardiomyocytes. Biophys J. 2007; 93:2581–95. [PubMed: 17545234]
45. Thul R, Smith GD, Coombes S. A bidomain threshold model of propagating calcium waves. J Math Biol. 2008; 56:435–63. [PubMed: 17786446]
46. Jafri MS, Keizer J. On the roles of Ca^{2+} diffusion, Ca^{2+} buffers, and the endoplasmic reticulum in IP_3-induced Ca^{2+} waves. Biophys J. 1995; 69:2139–53. [PubMed: 8580358]
47. Keizer J, Smith GD, Ponce-Dawson S, Pearson JE. Saltatory propagation of Ca^{2+} waves by Ca^{2+} sparks. Biophys J. 1998; 75:595–600. [PubMed: 9675162]
48. Fabiato A. Time and calcium dependence of activation and inactivation of calcium-induced release of calcium from the sarcoplasmic reticulum of a skinned canine cardiac Purkinje cell. J Gen Physiol. 1985; 85:247–89. [PubMed: 2580043]
49. Shannon TR, Ginsburg KS, Bers DM. Quantitative assessment of the SR Ca^{2+} leak-load relationship. Circ Res. 2002; 91:594–600. [PubMed: 12364387]
50. Loughrey CM, MacEachern KE, Cooper J, Smith GL. Measurement of the dissociation constant of Fluo-3 for Ca^{2+} in isolated rabbit cardiomyocytes using Ca^{2+} wave characteristics. Cell Calcium. 2003; 34:1–9. [PubMed: 12767887]
51. Sham JS, Cleemann L, Morad M. Functional coupling of Ca^{2+} channels and ryanodine receptors in cardiac myocytes. Proc Natl Acad Sci U S A. 1995; 92:121–5. [PubMed: 7816800]
52. Diaz ME, Trafford AW, O'Neill SC, Eisner DA. Measurement of sarcoplasmic reticulum Ca^{2+} content and sarcolemmal Ca^{2+} fluxes in isolated rat ventricular myocytes during spontaneous Ca^{2+} release. J Physiol. 1997; 501(Pt 1):3–16. [PubMed: 9174989]

53. Kubalova Z, Gyorke I, Terentyeva R, Viatchenko-Karpinski S, Terentyev D, Williams SC, Gyorke S. Modulation of cytosolic and intra-sarcoplasmic reticulum calcium waves by calsequestrin in rat cardiac myocytes. J Physiol. 2004; 561:515–24. [PubMed: 15486014]
54. Dawson SP, Keizer J, Pearson JE. Fire-diffuse-fire model of dynamics of intracellular calcium waves. Proc Natl Acad Sci U S A. 1999; 96:6060–3. [PubMed: 10339541]
55. O'Neill SC, Miller L, Hinch R, Eisner DA. Interplay between SERCA and sarcolemmal Ca^{2+} efflux pathways controls spontaneous release of Ca^{2+} from the sarcoplasmic reticulum in rat ventricular myocytes. J Physiol. 2004; 559:121–8. [PubMed: 15194743]
56. Lukyanenko V, Gyorke S. Ca^{2+} sparks and Ca^{2+} waves in saponin-permeabilized rat ventricular myocytes. J Physiol. 1999; 521(Pt 3):575–85. [PubMed: 10601490]
57. Stokke MK, Hougen K, Sjaastad I, Louch WE, Andersson KB, Christensen G, Eisner DA, Sejersted OM, Trafford AW. Ca^{2+} Wave Development in Ventricular Cardiomyocytes from Mice with Inducible Knockout of SERCA2. Biophys J. 2009; 96:275.
58. Sobie EA, Guatimosim S, Gomez-Viquez L, Song LS, Hartmann H, Saleet Jafri M, Lederer WJ. The Ca^{2+} leak paradox and rogue ryanodine receptors: SR Ca^{2+} efflux theory and practice. Prog Biophys Mol Biol. 2006; 90:172–85. [PubMed: 16326215]
59. Smith GL, O'Neill SC. A comparison of the effects of ATP and tetracaine on spontaneous Ca^{2+} release from rat permeabilised cardiac myocytes. J Physiol. 2001; 534:37–47. [PubMed: 11432990]
60. Gyorke S, Lukyanenko V, Gyorke I. Dual effects of tetracaine on spontaneous calcium release in rat ventricular myocytes. J Physiol. 1997; 500(Pt 2):297–309. [PubMed: 9147318]
61. Miura M, Boyden PA, ter Keurs HE. Ca^{2+} waves during triggered propagated contractions in intact trabeculae. Determinants of the velocity of propagation. Circ Res. 1999; 84:1459–68. [PubMed: 10381899]
62. Venetucci LA, Trafford AW, O'Neill SC, Eisner DA. The sarcoplasmic reticulum and arrhythmogenic calcium release. Cardiovasc Res. 2008; 77:285–92. [PubMed: 18006483]
63. Stern MD. The model of Snyder *et al.* does not simulate graded Ca^{2+} release from the cardiac sarcoplasmic reticulum in intact cells. Biophys J. 2000; 79:3353–4. [PubMed: 11203466]
64. Shannon TR, Guo T, Bers DM. Ca^{2+} scraps: local depletions of free [Ca^{2+}] in cardiac sarcoplasmic reticulum during contractions leave substantial Ca^{2+} reserve. Circ Res. 2003; 93:40–5. [PubMed: 12791706]
65. Rice JJ, Jafri MS, Winslow RL. Modeling short-term interval-force relations in cardiac muscle. Am J Physiol Heart Circ Physiol. 2000; 278:H913–31. [PubMed: 10710361]
66. Engel J, Sowerby AJ, Finch SA, Fechner M, Stier A. Temperature dependence of Ca^{2+} wave properties in cardiomyocytes: implications for the mechanism of autocatalytic Ca2+ release in wave propagation. Biophys J. 1995; 68:40–5. [PubMed: 7711265]
67. Soeller C, Crossman D, Gilbert R, Cannell MB. Analysis of ryanodine receptor clusters in rat and human cardiac myocytes. Proc Natl Acad Sci U S A. 2007; 104:14958–63. [PubMed: 17848521]
68. Hinch R, Greenstein JL, Tanskanen AJ, Xu L, Winslow RL. A simplified local control model of calcium-induced calcium release in cardiac ventricular myocytes. Biophys J. 2004; 87:3723–36. [PubMed: 15465866]

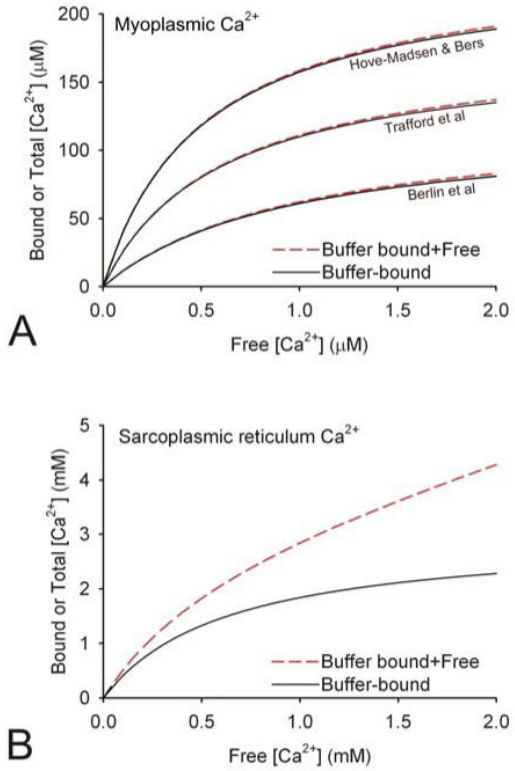

Figure 1.

Experimentally-derived Ca^{2+} buffering capacity curves for (A) myoplasm (13, 15, 16) and (B) SR (14). Continuous black curves denote buffer-bound Ca^{2+} and dashed red curves denote total Ca^{2+}. The marked difference between the three myoplasmic buffering curves may be accounted for by the time-frame within which buffering was measured. The lowest estimate (16) was obtained over a rapid time-scale and therefore represents fast buffering. The highest buffering capacity estimate (15) was determined over a much longer timescale and therefore also includes slow buffers.

Europe PMC Funders Author Manuscripts

Europe PMC Funders Author Manuscripts

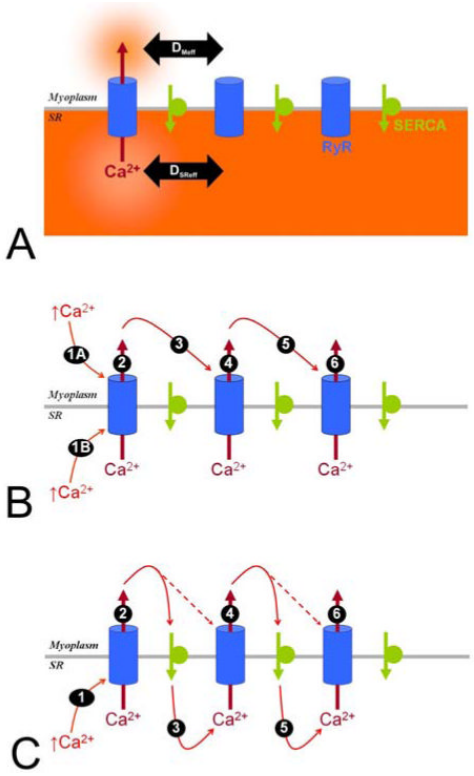

Figure 2.

Postulated mechanisms underlying Ca^{2+} waves. (A). Local Ca^{2+} release from the SR, through locally-activated RyRs, leads to a depletion of SR [Ca^{2+}] and a local rise in myoplasmic [Ca^{2+}]. The spatial influence of these two microdomains is set by the Ca^{2+} diffusion coefficient in myoplasm and SR (D_{Meff} and D_{SReff}). (B). The classical model for Ca^{2+} wave propagation postulates that the stimulus for RyR channel opening is myoplasmic [Ca^{2+}] (1A). An extension of this model takes into account modulation by the SR [Ca^{2+}] load. Under certain conditions, SR 'overload' can trigger RyR channel opening (1B). The myoplasmic microdomain of released Ca^{2+} spreads diffusively to adjacent RyRs and triggers their activation. This cycle repeats and a wave of Ca^{2+} release events propagates along the myocyte. (C). An alternative model for Ca^{2+} wave propagation. Ca^{2+} released from the SR through activated RyR channels is re-sequestered by SERCA pumps. The locally-elevated intra-SR [Ca^{2+}] spreads diffusively and sensitizes RyR channels en route. A rise in myoplasmic [Ca^{2+}] then readily activates sensitized RyR channels. The advancing myoplasmic Ca^{2+} wavefront therefore moves behind a wavefront of elevated (RyR-sensitizing) SR [Ca^{2+}]. For a wave to spread by this mechanism, intra-SR Ca^{2+} diffusion (3, 5...) cannot be slower than myoplasmic Ca^{2+} diffusion.

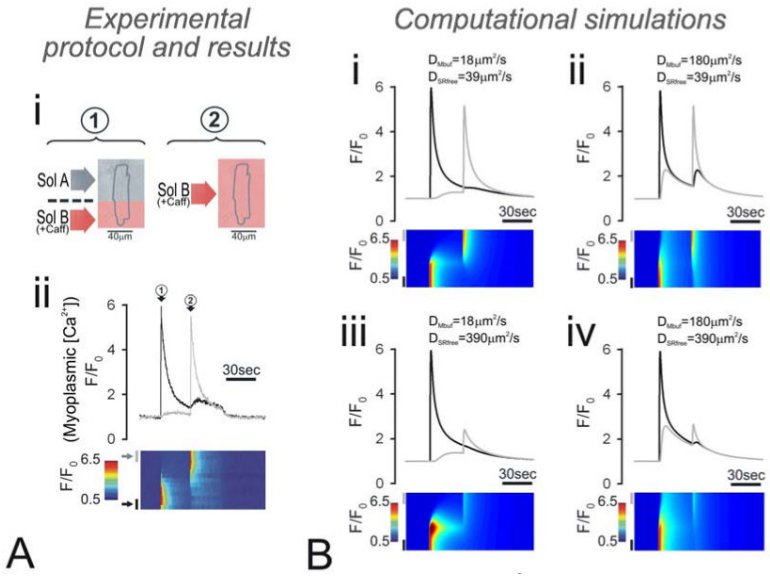

Figure 3.

(A) Experimental evidence for low myoplasmic and SR Ca^{2+} mobility. (i) Protocol based on (6) executed on a rat cardiac myocyte, preloaded with Fluo-3 to measure myoplasmic Ca^{2+} fluorescence F/F_0. (ii) F/F_0 was collected in linescan mode (bottom panel), normalized to cell-length along the y-axis. F/F_0 time-courses were sampled on either end of the myocyte, in regions of length equal to 20% of cell length (top panel). Protocol: myocyte was superfused with Na^+-free, Ca^{2+}-free (+0.5mM EGTA) solution to minimize sarcolemmal Ca^{2+} flux, with 10μM cyclopiazonic acid to block SERCA and 0.3mM tetracaine to block RyR channels ('solution A'). Arrow 1: One end of the myocyte was rapidly exposed to caffeine-containing 'solution B' (similar to 'solution A' but containing 10mM caffeine instead of tetracaine; caffeine-containing solutions have been shaded red). Remainder of the cell continued to be exposed to 'solution A'. This generated a regional and rapid release of Ca^{2+} from the caffeine-exposed SR into the myoplasm, which was recorded as a rise in normalized myoplasmic Fluo-3 fluorescence (F/F_0). Relaxation of F/F_0 back to 1 was mediated by the plasmalemmal Ca^{2+}-pump. The extent to which myoplasmic Ca^{2+} spread laterally was small, suggesting low Ca^{2+} mobility. Arrow 2: After a delay of 30s, the entire myocyte was bathed in 'solution B', thereby exposing the remainder of the myocyte to 10mM caffeine. This mobilized the remaining SR Ca^{2+}, which was recorded as a second rise in Fluo-3 fluorescence. The peak rise in F/F_0 was similar during the first and second caffeine maneuver. This indicates that SR Ca^{2+} diffusion was minimal. (B) Computational simulations for the experimental protocol with different diffusion coefficients for myoplasmic buffer mobility (D_{Mbuf}) and SR free Ca^{2+} mobility (D_{SRfree}): (i) 18 and 39μm^2/s, (ii) 180 and 39μm^2/s, (iii) 18 and 390μm^2/s, and (iv) 180 and 390μm^2/s. The best-fit is obtained with low myoplasmic and SR Ca^{2+} mobility.

Europe PMC Funders Author Manuscripts

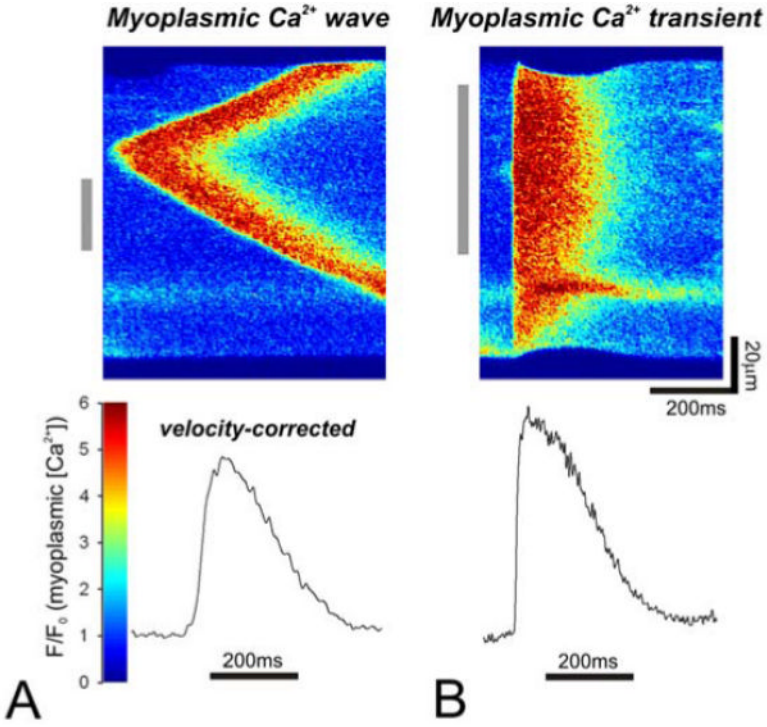

Figure 4.

Comparison of a myoplasmic Ca^{2+} wave and myoplasmic Ca^{2+} transient. A rat myocyte, bathed in normal Tyrode solution with elevated Ca^{2+} (7.5mM) to produce SR overload. Under these conditions, myocytes exhibit a high probability of firing Ca^{2+} waves. The linescans show Fluo-3 fluorescence (myoplasmic $[Ca^{2+}]$ signal) along a myocyte (y-axis) over time (x-axis). (A). Top: Around mid-length of the myocyte, a Ca^{2+} wave was triggered spontaneously, propagating along either sides of the myocyte at 89μm/s. Bottom: The velocity-corrected time-course of a fragment of the wave (indicated by the grey bar, left of linescan). (B). Top: The myocyte, bathed in the same solution, was field-stimulated to produce a Ca^{2+} transient. Bottom: The averaged time-course of a fragment of the transient (indicated by the grey bar, left of linescan).

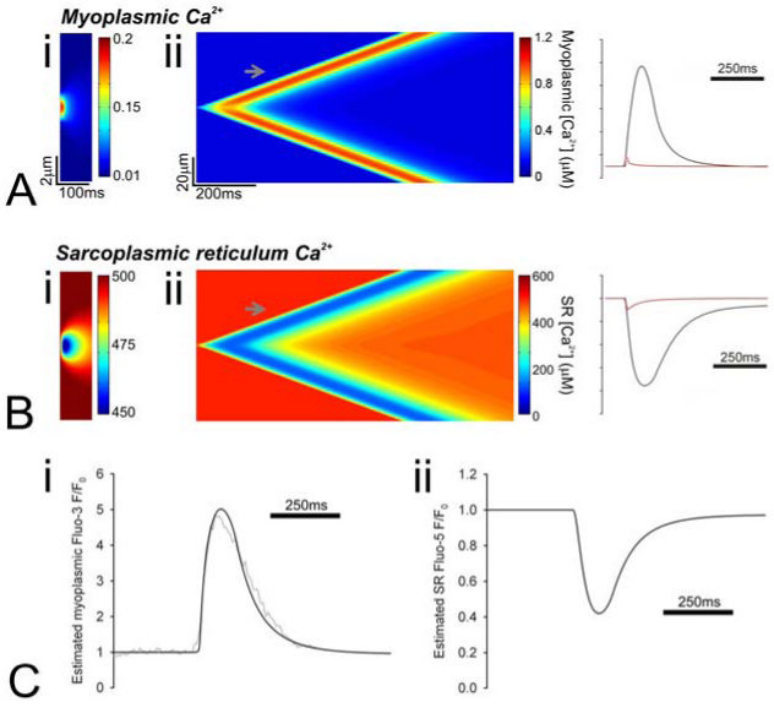

Figure 5.

Simulated Ca^{2+} in (A) the myoplasm and (B) SR. Ca^{2+} release from the SR was triggered by introducing an additional, exponentially decaying (time-constant 10ms) permeability (k_{act}) in the SR membrane in a 2μm-wide region mid-way along the model cell. (i) Below a critical level, k_{act} generates a unitary and isolated event that fails to propagate. This event is similar to a Ca^{2+} spark in myoplasm and a Ca^{2+} blink in the SR. (ii) Above a critical level, k_{act} triggers a Ca^{2+} wave that spreads to either end of the cell at 78μm/s. The time-plots (right) show the Ca^{2+} rise in myoplasm and the corresponding fall in the SR during the sub-threshold events (red trace) and during the triggered Ca^{2+} wave (black trace, plotted at the position indicated by the grey arrow on the linescans). (C) (i) Myoplasmic [Ca^{2+}] measured during a simulated Ca^{2+} wave was converted to Fluo-3 F/F_0 assuming a dye dissociation constant of 850nM. Superimposed on the prediction is the experimentally-determined Ca^{2+} wave time-course from Figure 4. (ii) SR [Ca^{2+}] measured during a simulated Ca^{2+} wave was converted to Fluo-5N F/F_0 assuming a dye dissociation constant of 400μM.

Europe PMC Funders Author Manuscripts

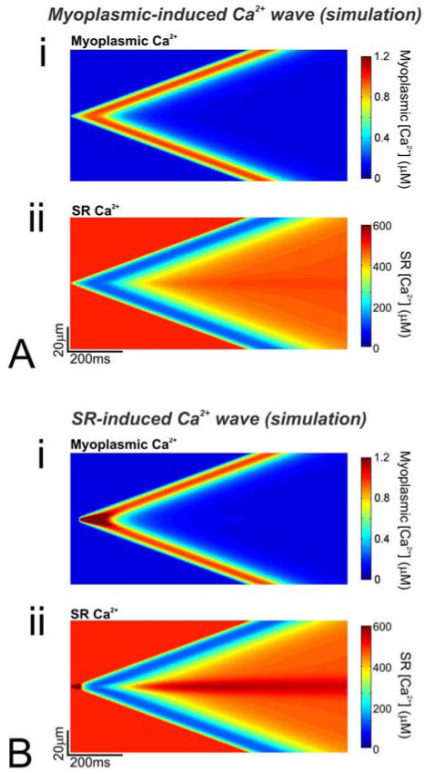

Figure 6.

(A) Simulated Ca^{2+} wave was triggered by raising myoplasmic Ca^{2+} locally (central 2μm region) above a critical level, beyond which local Ca^{2+} release is sufficiently large to open adjacent release sites in a propagating manner. Linescans for (i) myoplasmic and (ii) SR $[Ca^{2+}]$. (B) Simulated Ca^{2+} wave triggered by raising SR $[Ca^{2+}]$ locally (central 2μm region) to a level at which release occurs spontaneously at resting myoplasmic $[Ca^{2+}]$, i.e. the release threshold is lowered. Linescans for (i) myoplasmic and (ii) SR $[Ca^{2+}]$. Note that the wave velocity (78μm/s) is the same with both simulations. Also, the time-course of the myoplasmic and SR $[Ca^{2+}]$ are very similar (away from the trigger site).

Europe PMC Funders Author Manuscripts

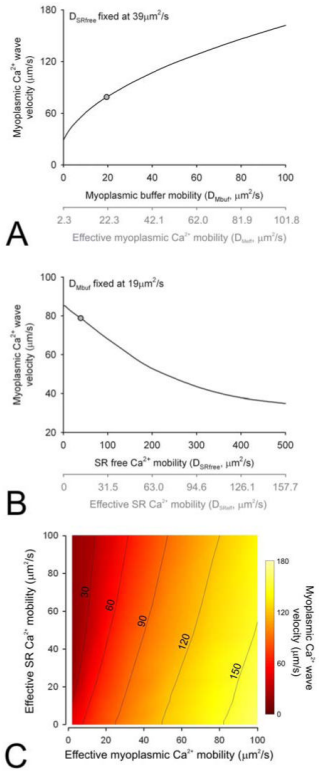

Figure 7.

(A) Simulated relationship between myoplasmic buffer mobility (D_{Mbuf}) and Ca^{2+} wave velocity, at fixed SR free Ca^{2+} mobility (D_{SRfree}=39μm^2/s). Grey circle: control conditions. (B) Simulated relationship between D_{SRfree} and Ca^{2+} wave velocity, at fixed D_{Mbuf}=18μm^2/s. Grey circle: control conditions. The triggering protocol is the same as in Figure 5. Also plotted in grey is a secondary axis with mobility converted to effective myoplasmic Ca^{2+} mobility (D_{Meff}) at 100nM and effective SR Ca^{2+} mobility (D_{SReff}) at half-filled SR. (C) Contour maps showing the relationship between wave velocity, D_{Meff} and D_{SReff}.

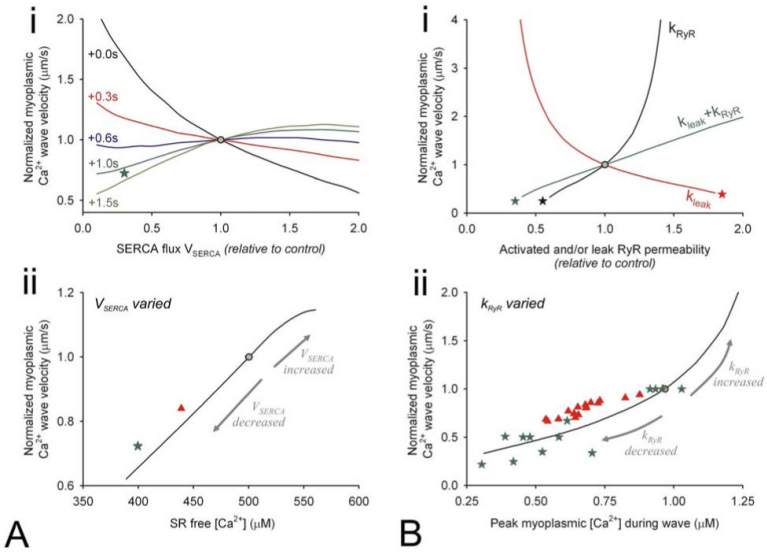

Figure 8.

(A) (i) Simulated relationship between control-normalized myoplasmic Ca^{2+} wave velocity and maximal SERCA flux (scaling V_{SERCA} by a factor of 0.2 to 2.0), calculated from myoplasmic Ca^{2+} waves triggered immediately after manipulation of V_{SERCA} or after a delay of 0.3, 0.6, 1s or 1.5s. D_{Mbuf}=18μm^2/s; D_{SRfree}=39μm/s. Grey circle: control conditions. Green star: data from Keller et al (41). (ii) Simulated relationship between control-normalized wave velocity and SR free $[Ca^{2+}]$. Different levels of SR load were obtained by varying V_{SERCA}. Grey circle: control conditions. Green star: data converted from Keller et al (41). Red triangle: data converted from Stokke et al (57). (B) (i) Simulated relationship between control-normalized myoplasmic Ca^{2+} wave velocity and RyR channel permeability. In one set of simulations (black curve), only activated RyR channel permeability (k_{RyR}) was varied, by scaling the control value by between 0.2 and 2.0. In a second set of simulations (red curve), leak RyR channel permeability (k_{leak}) was varied by scaling between 0.2 and 2.0 and allowing for the system to attain a new steady-state SR $[Ca^{2+}]$ load. In a third set of simulations, both parameters were varied simultaneously, and the system was allowed to attain a new steady-state (green curve). D_{Mbuf}=18μm^2/s; D_{SRfree}=39μm^2/s. Grey circle: control conditions. Stars indicate conditions at which waves fail to propagate. (ii) Simulated relationship between control-normalized wave velocity and peak Ca^{2+} amplitude, measured at 5μm away from trigger site, obtained by varying k_{RyR}. Grey circle: control conditions. Green stars: data from Trafford et al (39). Red triangles: data from Smith & O'Neill (59).

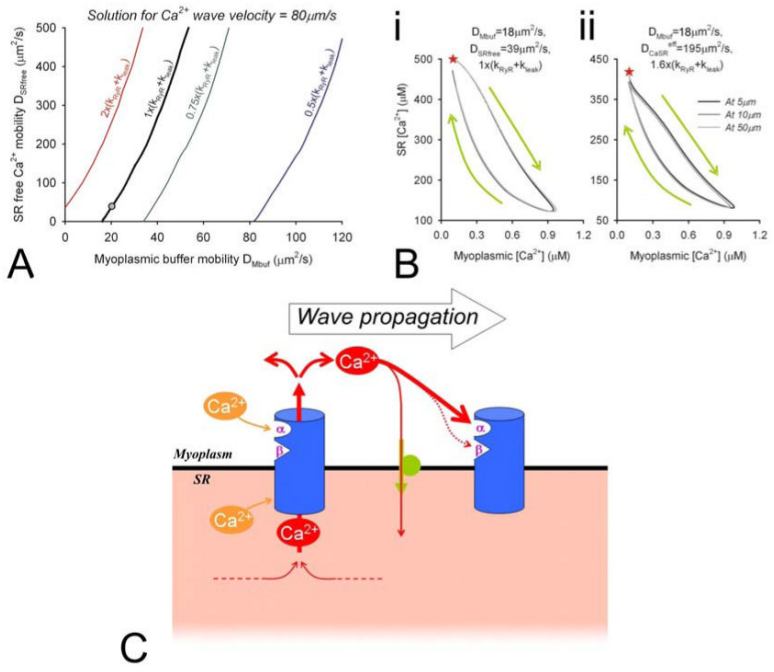

Figure 9.

(A) Solution curves for the combination of D_{SRfree}, D_{Mbuf} and $k_{RyR}+k_{leak}$ that predict wave velocity of 78μm/s. (B) Hysteresis loops for myoplasmic $[Ca^{2+}]$ versus and SR $[Ca^{2+}]$ during a Ca^{2+} wave, plotted at 5, 10 and 50μm away from the midpoint of the cell (trigger site). Green arrows indicate direction of hysteresis. Red stars indicate the start of the hysteresis. The model was parameterized to give a wave velocity of 78μm/s. (i) Hysteresis loop obtained for a Ca^{2+} wave under conditions of low Ca^{2+} mobility (D_{Mbuf}=18μm^2/s, D_{SRfree}=39μm^2/s) at control $k_{RyR}+k_{leak}$. (ii) Hysteresis loop obtained for a Ca^{2+} wave under conditions of high SR Ca^{2+} mobility (D_{SRfree}=195μm^2/s) with 1.6-fold higher $k_{RyR}+k_{leak}$ to yield the desired 78μm/s wave velocity. In all cases, the hysteresis is clockwise, indicating that the rise in myoplasmic $[Ca^{2+}]$ was not preceded by a rise in SR $[Ca^{2+}]$. NB: hysteresis was not due to buffering, as this was fast. (C) Proposed model for Ca^{2+} wave propagation, inferred from comparing experimental data with the present mathematical modeling. RyR channels (blue icon) contain two myoplasmic Ca^{2+}-sensitive 'gates': α (fast activation) and β (slow inactivation) and an inhibitory, SR-facing calsequestrin-sensitive site. To trigger the wave, Ca^{2+} occupancy of β cannot exceed that of α. Once RyR channel is open, the magnitude of Ca^{2+} release depends on RyR permeability, the transmembrane $[Ca^{2+}]$ gradient and the volume over which SR $[Ca^{2+}]$ is drawn by diffusive dissipation (i.e. D_{SReff}). Ca^{2+} diffusion within the SR will affect the substrate for Ca^{2+} release and calsequestrin-RyR interaction elsewhere in the SR. In the myoplasm, the spatial spread of released Ca^{2+} will be determined by Ca^{2+} diffusion (D_{Meff}) and uptake by SERCA pumps (green icon). If a supra-threshold myoplasmic $[Ca^{2+}]$ is delivered to an adjacent, activatable RyR channel (site α occupancy>site β occupancy) and if SR $[Ca^{2+}]$ is sufficiently high to provide release substrate and sufficiently low to maintain low (calsequestrin) locally, Ca^{2+} will flux out of the SR. A Ca^{2+} wave is propagated.

Europe PMC Funders Author Manuscripts

Europe PMC Funders Author Manuscripts

Table 1

Constants used for simulating Ca^{2+} waves

Symbol	Parameter description	Value
v_{myo}	Volume fraction of myoplasm (6, 38)	0.65
v_{SR}	Volume fraction of SR (6, 38)	0.035
C_{mbuf}	Myoplasmic buffer concentration (6, 13)	175μM
K_{mbuf}	Myoplasmic buffer dissociation constant (6, 13)	590nM
k_m	Myoplasmic buffer on rate constant *	100/μM/s
C_{SRbuf}	SR buffer concentration (6, 14)	4.0mM
K_{SRbuf}	SR buffer binding constant (6, 14)	630μM
k_{SRbuf}	SR buffer on rate constant *	100/μM/s
V_{SERCA}	Maximum flux on SERCA (14, 38)	500μM/s
δ	Max SR/myoplasm $[Ca^{2+}]$-gradient (14, 38)	7000
K_{SERCA}	SERCA Ca^{2+} dissociation constant (14, 38)	0.25μM
V_{NCX}	Maximum flux on NCX (38)	1.2mM/s
K_{NCX}	NCX Ca^{2+} dissociation constant (38)	36μM
k_{sl}	Sarcolemmal leak rate constant#	0.0033/s
k_{leak}	Background RyR channel flux constant at filled SR, scaled to fit leak-loak data (49)#	0.063/s
k_α^+	S_α on-rate constant	Not limiting
k_α^-	S_α off-rate constant	Not limiting
k_β^+	S_β on-rate constant at loaded SR $[Ca^{2+}]$=500μM#	5/μM/s
k_β^-	S_β off-rate constant#	0.59/s
k_{RyR}	Activated RyR channel flux constant#	18/s
D_1	Free Ca^{2+} diffusion coefficient in myoplasm	500μm^2/s
D_2	Ca^{2+}-bound myoplasmic buffer diffusion coefficient	18μm^2/s
D_3	Unbound myoplasmic buffer diffusion coefficient	18μm^2/s
D_4	Free Ca^{2+} diffusion coefficient in SR	39μm^2/s

Symbol	Parameter description	Value
D_5	Ca^{2+}-bound calsequestrin diffusion coefficient	0 $\mu m^2/s$
D_6	Unbound calsequestrin diffusion coefficient	0 $\mu m^2/s$

* parameter assumed to be diffusion-limited

parameter best-fitted to data

Europe PMC Funders Author Manuscripts